Universidade de Aveiro Departamento de Biologia
2016

JOSÉ CARLOS RIBEIRO FERREIRA PEREIRA

REGULAÇÃO DO CITOESQUELETO NAS CÉLULAS DO CANCRO DA BEXIGA APÓS TRATAMENTO FOTODINÂMICO

CYTOSKELETON REGULATION IN BLADDER CANCER CELLS AFTER PHOTODYNAMIC TREATMENT

DECLARAÇÃO

Declaro que este relatório é integralmente da minha autoria, estando devidamente referenciadas as fontes e obras consultadas, bem como identificadas de modo claro as citações dessas obras. Não contém, por isso, qualquer tipo de plágio quer de textos publicados, qualquer que seja o meio dessa publicação, incluindo meios eletrónicos, quer de trabalhos académicos.

Universidade de Aveiro Departamento de Biologia
2016

JOSÉ CARLOS RIBEIRO FERREIRA PEREIRA

REGULAÇÃO DO CITOESQUELETO NAS CÉLULAS DO CANCRO DA BEXIGA APÓS TRATAMENTO FOTODINÂMICO

CYTOSKELETON REGULATION IN BLADDER CANCER CELLS AFTER PHOTODYNAMIC TREATMENT

Dissertação apresentada à Universidade de Aveiro para cumprimento dos requisitos necessários à obtenção do grau de Mestre em Biologia Molecular e Celular, realizada sob a orientação científica da Doutora Rosa Cristina Simões Fernandes, Investigadora Auxiliar do Instituto da Imagem Biomédica e Ciências da Vida - Faculdade de Medicina da Universidade de Coimbra e co-orientação do Professor Doutor João Paulo Costa Tomé, Professor Associado do Departamento de Engenharia Química do Instituto Superior Técnico da Universidade de Lisboa

This work was conducted at the Institute for Biomedical Imaging and Life Sciences (IBILI), Faculty of Medicine, University of Coimbra.

This work was primarily supported with funds from the Foundation for Science and Technology (Strategic Projects PEst-C/SAU/UI3282/2011-2013, UID/NEU/04539/2013, FCT UID/QUI/00062/2013 and FCT UID/QUI/0100/2013), Portugal and COMPETE/ FEDER.

Dedico este trabalho ao meu pai que partiu e por tudo que me ensinou, à minha mãe pela força que me dá e à minha querida irmã Margarida. Vocês são o que me dá forças para continuar.

“One's work may be finished someday,

but one's education never”

Alexandre Dumas

o júri

presidente

Professora Doutora Maria Helena Abreu Silva
Professora Auxiliar do Departamento de Biologia da Universidade de Aveiro

Doutora Rosa Cristina Simões Fernandes
Investigadora Auxiliar da Faculdade de Medicina da Universidade de Coimbra

Doutor Flávio Nelson Fernandes Reis
Investigador Auxiliar da Faculdade de Medicina da Universidade de Coimbra

agradecimentos

Finalmente acabo o meu mestrado, e relembro com saudades os tempos desde a minha licenciatura quando entrei na Universidade do Porto, os meus tempos no mestrado quando fui para a Universidade de Aveiro, e finalmente agora acabando a desenvolver o meu trabalho na Universidade de Coimbra. Tem sido uma viagem em tanto. Assim, tenho de expressar a minha gratidão a todos aqueles que nas diversas fases da minha vida me ajudaram a avançar:

À Doutora Rosa Fernandes, por me ter permitido trabalhar no seu grupo de investigação, pela orientação que prestou durante o meu tempo em Coimbra e pela oportunidade que me deu na realização deste trabalho. Agradeço ainda pela disponibilidade concedida, pela liberdade dada para realizar as experiências, por todas as horas despendidas comigo para tornar este trabalho possível e pela confiança depositada em mim. Espero que continue a ter muito sucesso.

Ao Professor Doutor João Tomé pela sua coorientação, disponibilidade, auxílio e palavras de incentivo para a realização deste trabalho. Desejo-lhe as melhores felicidades no seu caminho.

À Doutora Patrícia Pereira pela ajuda e disponibilidade desde o inicio, por me ter ensinado o que precisava de saber no laboratório, pelo auxílio prestado em tudo que precisava, pela amizade e por tudo quanto me ensinou, um especial obrigado.

Agradeço a todas as pessoas do IBILI e CNC que me ajudaram ao longo deste ano, não só no laboratório, mas pela companhia, em especial à Ana Peixoto, à Andreia Gonçalves, à Cátia Sousa, à Daniela Oliveira, à Inês Pita, à Isabel Ferreira, à Joana Teles, ao Luís António, à Cristhyane Costa, à Manuela Meireles, à Marina Couto, ao Ricardo Leitão, à Sara Carolina Rodrigues, à Sara Nunes e à Vanessa Santos.

À Débora Serrenho pela amizade, companhia e conselhos, obrigado pela tua boa disposição e pelas nossas longas conversas filosóficas.

Aos meus amigos de Mestrado em Biologia Molecular e Celular por fazerem parte da minha vida, ao André Gabriel, à Bibiana Costa, à Emilie Pinheiro, à Inês Sardo, à Mónica Oliveira e à Rita Almeida pelo companheirismo, amizade, e pelo apoio em todos os momentos que precisei. Obrigado por serem incríveis.

Aos meus grandes amigos e confrades João Reis e Mário Dias, pelos momentos de zoeira e companheirismo, que a nossa amizade dure muitos e longos anos.

Um agradecimento geral ao pessoal do FMC pelas distrações, incentivos e secretárias mandadas a voar, nunca mudem.

À minha Família, ao meu pai que me ensinou tanto, à minha mãe e minha irmã que são as pessoas mais importantes da minha vida, que me acompanharam desde sempre. Espero um dia poder retribuir a alegria que me deram e continuam a dar.

Um obrigado a todos aqueles que se opuseram a mim e tentaram deitar-me abaixo. A raiva que graças a vós nasceu deu-me a força para não ficar mais parado e enfrentar o que cada dia tinha para dar e proteger o que me era querido.

Um obrigado final a todos que se cruzaram comigo ao longo da minha vida e ajudaram a fazer de mim a pessoa que sou hoje.

palavras-chave

Terapia Fotodinâmica, $PorGal_8$, Citoesqueleto, Filamentos de Actina, Filamentos Intermédios, Microtubúlos, RhoA

resumo

A terapia fotodinâmica (PDT) é uma modalidade promissora para o tratamento do cancro. Esta terapia baseia-se na interação entre um composto químico (fotossensibilizador, PS), luz com um determinado comprimento de onda e oxigénio molecular para originar a produção de espécies reativas de oxigénio (ROS). Devido à sua elevada reatividade, estas espécies tóxicas podem causar danos severos conduzindo à morte celular. Atualmente, os PS disponíveis na clínica para o tratamento de tumores apresentam baixa seletividade para as células tumorais. Estudos anteriores do nosso grupo descreveram uma porfirina conjugada com unidades dendríticas de galactose ($PorGal_8$) como um novo PS solúvel em solução aquosa, capaz de gerar ROS após fotoativação e com reconhecimento por parte de proteínas (galectina-1) que se encontram sobreexpressas nas células do cancro da bexiga. Vários estudos têm descrito alterações no citoesqueleto em resposta ao tratamento fotodinâmico. No entanto, a contribuição da desorganização do citoesqueleto na morte celular induzida por PDT encontra-se pouco esclarecida.
Neste trabalho, avaliámos de que forma alterações nos constituintes do citoesqueleto – filamentos de actina, filamentos intermédios e microtúbulos – estão relacionadas com morte celular induzida por PDT com $PorGal_8$.
O uptake de $PorGal_8$ em duas linhas celulares do cancro da bexiga derivadas de carcinoma de células transicionais (UM-UC-3 e HT-1376), foi dependente da concentração. O uptake celular de $PorGal_8$ foi superior nas células UM-UC-3, que exibem níveis superiores da proteína galectina-1, comparativamente com as células HT-1376. $PorGal_8$ mostrou não ser tóxico no escuro. A fotoativação da $PorGal_8$ resultou numa fototoxicidade significativamente superior nas células UM-UC-3 relativamente às células HT-1376. A $PorGal_8$ não induziu alterações significativas nos níveis de proteína α-tubulina nas células UM-UC-3. No entanto, observou-se uma redução significativa nos níveis de α-tubulina nas células HT-1376 vinte e quatro horas após tratamento com irradiação. Apesar de se ter observado uma recuperação na organização dos microtúbulos em algumas células, a intensidade da fluorescência diminuiu consideravelmente na maior parte das células HT-1376. Uma redução significativa nos níveis de proteína dos filamentos intermédios (vimentina) foi observada em ambas as linhas celulares vinte e quatro horas após irradiação. Trinta minutos após a irradiação, as células UM-UC-3 e HT-1376 apresentaram uma clara retração nos filamentos de actina com perda de fibras de stress. Ao contrário das células UM-UC-3 em que não se verificaram sinais de recuperação, em algumas células HT-1376 verificou-se uma certa reorganização dos filamentos de actina, com curtas fibras de stress, longas extensões, grandes filopodia, o que parece sugerir uma possível recuperação das células HT-1376. A RhoA, uma proteína da família de pequenas proteínas GTPases, descrita como estando relacionada com a expressão da galectina-1, foi adicionalmente avaliada. Resultados preliminares indicaram que a $PorGal_8$ induziu uma tendência para aumentar os níveis de RhoA nas células HT-1376 vinte e quatro horas após tratamento com irradiação.
Concluindo, os nossos resultados contribuem para o esclarecimento dos mecanismos subjacentes dos efeitos fototóxicos da $PorGal_8$. Uma melhor compreensão dos intervenientes e das alterações induzidas imediatamente após PDT nas estruturas do citoesqueleto em cancros resistentes à terapia, poderão contribuir para o desenvolvimento de novos agentes terapêuticos adjuvantes à PDT.

keywords

Photodynamic Treatment, $PorGal_8$, Cytoskeleton, Actin Filaments, Intermediate Filaments, Microtubules, RhoA

abstract

Photodynamic therapy (PDT) is a promising modality for the treatment of cancer that involves light of an appropriate wavelength and a photosensitizing drug (photosensitizer, PS), used in conjunction with molecular oxygen, leading to the production of reactive oxygen species (ROS). In a biological environment, these toxic species can interact with the cellular constituents eliciting cell death. Currently, the PS available show poor tumor specificity. Previous work from our research group reported a porphyrin conjugated with dendritic units of galactose ($PorGal_8$) as a new water soluble PS, able to generate ROS after photoactivation and exhibiting increased selectivity to bladder cancer cells overexpressing galectin-1. Several studies reported cytoskeleton alterations derived from photodynamic treatments. However, the role of cytoskeleton disorganization in cell death induced by PDT remains unclear.

In this work we evaluated whether changes in the cytoskeletal constituents - actin filaments, intermediate filaments and microtubules - are correlated with cell death triggered by PDT with $PorGal_8$.

The uptake of $PorGal_8$ in two bladder cancer lines derived from transitional cell carcinoma (UM-UC-3 and HT-1376 cells), was concentration dependent. Cellular uptake of $PorGal_8$ was higher in UM-UC-3 cells that express higher levels of galectin-1 protein than HT-1376 cells. $PorGal_8$ was nontoxic in dark. Photoactivation of PorGal8 resulted in a significantly higher phototoxicity in UM-UC-3 cells than HT-1376 cells. $PorGal_8$ did not change the α-tubulin protein levels in UM-UC-3 cells but reduced α-tubulin twenty-four hours after photodynamic activation in HT-1376 cells. Although a few cells showed a recovery in microtubules organization, the fluorescence intensity decreased noticeably in most of the HT-1376 cells. A significant decrease in intermediate filaments (vimentin) protein levels was exhibited in both cell lines twenty-hours after irradiation. Thirty minutes post-irradiation, UM-UC-3 and HT-1376 cells showed a clear retraction of actin filaments with loss of stress fibers. Although no recovery was observed in UM-UC-3 cells, some cells present some reorganization in actin filaments, presenting short stress fibers, long extensions, like large filopodia, suggesting a possible recovery in HT-1376 cells. A small GTPases family protein, RhoA, referred to be involved with galectin-1 expression, was also evaluated, with preliminary results indicating a tendency towards an increase in HT-1376 cells twenty-four hours after therapy. Overall, our results give new insights into the mechanisms underlying the phototoxic effects of $PorGal_8$. Better understanding the intrinsic web of events and alterations on cytoskeleton structures induced immediately after photodynamic treatment in resistant cancers may contribute to envisage new potential therapeutic adjuvants for PDT.

Contents

Abbreviation and Acronyms

ALA	5-aminolevulinic acid
AMD	Age-related Macular Degeneration
BCA	Bicinchoninic Acid
BSA	Bovine Serum Albumin
CIS	Carcinoma in situ
DAPI	4′,6-Diamidino-2-phenylindole
DMSO	Dimethyl Sulfoxide
DTT	Dithiothreitol
GLUT-1	Glucose Transporter 1
EGTA	Ethylene glycol-bis(β-aminoethyl ether)-N,N,N',N'-tetraacetic acid
HpD	Hematoporphyrin Derivate
ICC	Immunocytochemistry
IF	Intermediate Filaments
MTT	3-[4,5-dimethylthiazol-2-yl]-2,5-diphenyl-tetrazolium bromide
OVNA	Sodium orthovanadate
PBS	Phosphate-buffered saline
PDT	Photodynamic Therapy
PFA	Paraformaldehyde
PMSF	Phenylmethane sulfonyl fluoride
PS	Photosensitizer
^{1}PS	Photosensitizer in the ground-state
^{1}PS*	Photosensitizer in the excited-singlet-state
^{3}PS*	Photosensitizer in the triplet excited state
PVDF	Polyvinylidene fluoride
PorGal$_8$	Galactodendritic Porphyrin
RIPA	Radio immunoprecipitation assay
RT	Room Temperature
RhoA	Ras homolog gene family, member A
ROS	Reactive Oxygen Species
S.E.M.	Standard Error of Mean
SDS	Sodium Dodecyl Sulfate
WB	Western Blotting

Table of Figures

Table of Tables

Chapter 1. Introduction

1.1 Bladder Cancer

Bladder cancer has become a common malignancy worldwide, with an estimated 430,000 new cases diagnosed in 2012 (Ferlay et al. 2013), and it is characterized by a high recurrence rate.

Bladder cancer has higher prevalence in men than in women. The incidence and mortality rates per 100,000 in the European Union are 14.4 and 4.5, respectively, being the fifth most common type of cancer among men in Portugal. It is estimated that in Portugal the number of new cases 23,400 for males and 5,400 for females; cancer deaths due to bladder cancer are 6,600 for males and 2,000 for females (Ferlay et al. 2013). Although the improvement in medical care and prevention, it is still a widely spread disease worldwide, with incidence and mortality variable across countries and between sexes. Bladder cancer is mostly diagnosed in patients over 50 years old, although it can manifest at any age. Most of the patients diagnosed with bladder cancer remain non-muscle invasive or superficial (Bryan et al. 2010). Although the existing data for recurrence after treatment of bladder cancer are conflicting, variating from 15% to 80% at 1 year, some aspects are known: bladder cancer re-incidence tends to increase from 1 to 5 years after treatment and most of the patients that present recurrence will develop distant metastases (Soukup et al. 2012; Van Den Bosch & Witjes 2011).

The bladder is a hollow organ shaped like a balloon located in the lower abdomen just above and behind the pelvic bone. Due to its main function (urine storage), it has muscular and flexible walls. The urinary bladder wall is lined with transitional cells (transitional epithelium or urothelium) and squamous cells. Next to urothelium is a layer of loose connective tissue, called lamina propria, which is covered by three indistinctively separated layers of smooth muscle. Outside these three layers is a fat layer that lines and protects the bladder (Fig. 1) (Assefa & Yosief 2003; Saladin 2008).

Bladder cancer progression is characterized by four stages (Fig. 1). The stage of a bladder cancer describes how far it has spread. It can be confined to the lining of the bladder (early stage) or it can spread to lymph nodes near the bladder or spread to nearby organs (invasive).

Stage 0 tumors arising in the urothelium can spread to the lamina propria layer (stage I). Until this degree they are called superficial bladder cancers or non-muscle invasive. As cancer grows and invades the muscle layer of the bladder wall originates a muscle invasive cancer (stage II). It can further extend beyond the bladder muscle and into the outer layer (stage III) or further spreading toward the abdominal or pelvic wall (stage IV). Muscle invasive cancers after stage IV

may start to invade nearby organs, usually the uterus or vagina in women or the prostate gland in men, and possibly invade the wall of the abdomen. At this point, when bladder cancer invasiveness is at its maximum, cancer cells can start to be found in nearby lymph nodes as in other organs. This process of invasion of other organs from the original place/organ is called metastasis (Bryan et al. 2010; Park et al. 2014).

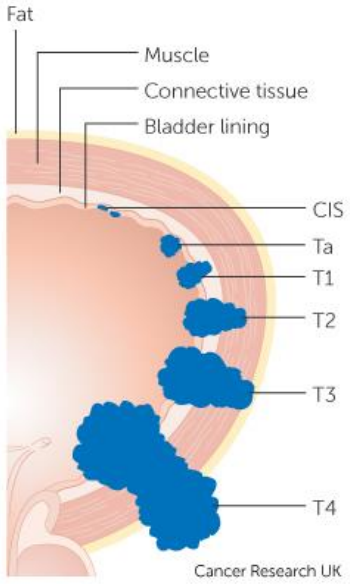

Figure 1. Bladder layers and bladder cancer progression (non-invasive tumours: stages CIS, Ta and T1; invasive tumours: T2-4) Adapted from (http://www.cancerresearchuk.org/)

The most commonly used system of classification of tumor penetration degree is the American Joint Committee on Cancer (AJCC) Tumor-Node-Metastases system (TNM) based in three key categories (T, N and M) subdivided according to invasiveness. In either stage X represents lack of information to be assessed a diagnostic, and 0 absence of cancer to those categories. According to this classification system, T describes how far the primary tumor has grown, being a Ta a non-invasive papillary carcinoma, low grade tumors; and a Tis being a high grade non-invasive flat carcinoma (flat carcinoma in situ, or CIS). Tis are difficult to remove and if left untreated will progress to muscle invasive. When it progresses to the lamina propria it is then classified as a T1. After invading the muscle layer, it is a T2 tumor, subdivided in T2a and T2b if it has grown to the inner or outer half of the muscle layer, respectively. After invading the fat layer surrounding the bladder is classified as a T3, if only visible microscopically a T3a, or if large enough to be seen or sensed by a surgeon or medical imaging. Further progress to the surrounding organs is categorized as T4, further divided as a T4a when spreading to prostate

(men) or to the uterus and/or vagina (women), or as a T4b when spreading to the pelvic or abdominal walls. N categories describes spreading only to near lymph nodes, being divided in N1 to a single lymph node affected in the pelvis, N2 to two or more affected lymph nodes, and N3 when the cancer spreads to lymph nodes along the iliac artery. The final categorizing stage M represents the absence, M0, or presence, M1, of metastasis in other places/organs (Bryan et al. 2010; Park et al. 2014; Tanaka et al. 2011; Thompson et al. 2015; Egner 2010).

Combining these categories (T, N and M) and bladder cancer stages (I to IV), the overall cancer stage can be determined. The main overall stages are 0a (Ta, N0, M0); 0is (Tis, N0, M0); stage I (T1, N0, M0); stage II (T2a or T2b, N0, M0); stage III (T3a, T3b or T4a, N0, M0). Stage IV is composed of any cancer T4b and/or since the cancer starts invading nearby lymph nodes or metastasis to other parts of the body (Egner 2010).

The most common treatment for bladder cancer is transurethral resection and intravesical therapy. Cystoscopy, urine cytology, excretory urograms and medical imaging as used for bladder cancer diagnosis. However, the success in the immediate treatment of these disease is overshadowed by the high recurrence rates and tumor understaging, many times due to ineffective or incorrect performed surgery and tumor evaluation (Bryan et al. 2010; Soukup et al. 2012; Van Den Bosch & Witjes 2011).

1.1.1 Bladder cancer treatment

The conventional treatments of bladder cancer include radical cystectomy and transurethral resection, followed by radiation therapy and systemic chemotherapy (trimodality therapy). Radical cystectomy has been considered the gold-standard treatment for muscle-invasive bladder cancer and involves removal of the bladder and prostate in men and anterior exenteration (bladder, uterus, ovaries, and part of vagina) for women (Chedgy et al. 2016). Combined treatment approaches comprising transurethral resection of the bladder tumor and intravesical therapy present a compelling alternative to radical cystectomy (Bekelman et al. 2013). However, these conventional approaches might cause unwanted side effects and in some cases they are not totally effective (Witjes et al. 2010). Therefore, there is a pressing need for the development of anticancer drugs targeting the bladder cancer cells, while sparing normal surround tissue and limiting side effects.

1.2 Photodynamic Treatment (PDT)

Photodynamic Therapy (PDT) is a therapeutic approach that involves three main components: a non-toxic photo active drug called photosensitizer (PS), a harmless light source with particular wavelength, and the production of reactive molecular oxygen in the target tissue (Castano et al. 2004). After selective accumulation in cancer cells, irradiation of the tumor with a light source with specific wavelength induces the excitation of the PS from a ground-state to an excited singlet state, $^{1}PS^{*}$. The excited-singlet-state has a very low half-life time (between 10^{-6} seconds and 10^{-9} seconds), being extremely unstable, which can decay back to the its ground-state emitting fluorescence (Celli et al. 2003). However, the PDT effect is obtained when $^{1}PS^{*}$ undergoes intersystem crossover to an electronically different excited state, the excited-triplet state, $^{3}PS^{*}$ (Fig. 2) (Calin & Parasca 2006; Luksiene 2003). As $^{3}PS^{*}$ has longer life time than the singlet-state, the cytotoxic effects of PDT are usually mediated by that state. $^{3}PS^{*}$ can either directly react with the substrate creating radical ions that will interact with molecular oxygen producing reactive oxygen species (type I reaction) or react with the surrounding molecular oxygen producing a reactive cytotoxic form of oxygen, singlet oxygen (type II reaction) as the primary photochemical product (Castano et al. 2004; Foote 1991; Celli et al. 2003). Type-I photochemical reactions often result in the formation of superoxide anion by the transfer of an electron from the PS to molecular oxygen. Although superoxide anion is not a very reactive oxygen species in biological systems, it can react to induce hydrogen peroxide (H_2O_2) production, which can easily cross biological membranes, inducing cellular damage (Bergamini et al. 2004; Sharman et al. 2000).

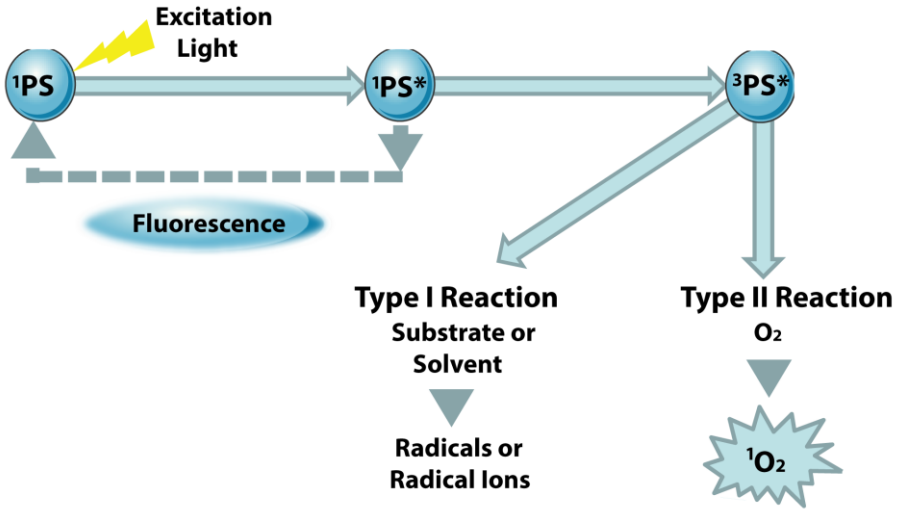

Figure 2. PDT Principle under photo-physical and -chemical points of view

In order to ensure adequate PS excitation and tissue penetration, it is essential to choose a suitable source for PDT. Wavelengths in the visible light, between 400 and 800 nm, can induce relevant cellular responses to PDT (Celli et al. 2003). Due to blue light penetrates less efficiently through tissue than red and infrared radiations, the maximum absorption of the PS for PDT should correspond to the window between 650-850 nm, where penetration of light into tissue is quite high and the energy of the triplet state is enough for singlet oxygen production (Plaetzer et al. 2009).

First reports of the PDT principle have been found to date back as much as 3,500 years ago in ancient cultures such as in Egypt, Greece and India, were a mixture of herbs followed by exposure to sunlight was used to treat many skin diseases such as skin depigmentation. These reports can be found around ancient cultures, but PDT as a treatment practically disappeared from the world since ancient times having remerged in the final 1890, early 1900. Since then PDT has been found to be a viable treatment to various maladies: acne, wet age-related macular degeneration (AMD), psoriasis, herpes, malignant forms of cancer in bladder, lungs, head, neck and particularly skin. Its first use in the treatment of cancer was described in 1903 by von Tappeiner and Jesionek were preliminary results using eosin applied to basal carcinoma cells prior to irradiation (Jodlbauer & Von Tappeiner 1904). In parallel, in 1913, Meyer-Betz started studying a class of PS called porphyrins, using the substance Hematoporphyrin to treat rat tumours and going as far as self-administrate and expose the administrated area to sun light resulting in swelling and burning sensation due to phototoxic reaction induced by the activation of the PS (Meyer-Betz 1913).

Compared to other forms of treatment, PDT is a preferable treatment to various maladies. In bladder cancer for example, due to its translucent tissue, geometry, allowing symmetrical light distribution, and easy access through endoscopy associated with newer light delivery catheters, bladder is an organ that possesses a high potential to be a suitable target for this therapy, in opposition to currently existing therapies that have higher risks. Nevertheless, PDT has its disadvantages. The promising use of PDT in order to cure a panoply of diseases has instigated its research in order to improve it in order to be used as a viable and more widely spread therapy (Luksiene 2003).

Since its first medical application in the treatment of cancer, a continuous struggle has been fought in order to found better and powerful PSs that could gather the desirable characteristics to pharmaceutical administration and safely used in human cancer treatment. In

this field, researchers continuously try to design and synthesize new PSs as potential therapeutic agents in cancer treatment. However, to date, none of the PS available on the market exhibit only accumulation in the cancer cells, and their uptake by non-cancerous cells cannot completely be avoided (MacDonald & Dougherty 2001). Therefore, the choice of a suitable PS, along with a compatible light source are key components in PDT.

The development of an "ideal" PS for PDT should meet the following criteria (Pushpan et al. 2002): (i) available in pure form with known chemical composition; (ii) photostable and soluble in aqueous media; (iii) strong absorption in the red region of the electromagnetic spectrum (680-800 nm); (iv) lack of dark toxicity of the PS and its metabolites; (v) high phototoxicity via high singlet oxygen quantum yield; (vi) specific accumulation in cancer cells; (vi) easy administration; (vii) rapid elimination (pharmacokinetics) after PDT application, in order to minimize the risk of photosensitivity or other unwanted secondary effects. The specific nature of an ideal photosensitizer instigates research in order to create the best ones.

1.2.1 First, second and third generation PSs

Due to number of characteristics that an ideal PS must possess, different kinds of PSs have been developed over the years. PSs can be divided in first, second and third-generation PSs. The great majority of these pharmaceuticals are either porphyrin, derivatives or related compounds. Porphyrins are heterocyclic macrocycle organic compounds with an aromatic ring that can be naturally found, one of the most well-known examples is heme, co-factor of hemoglobin that gives the pigmentation to red blood cells. The absorption spectra of these compounds is composed of one strong absorption band, called Soret band (around 400 nm) and four progressively smaller bands, called Q bands, for the free base derivatives (Bonnett & Berenbaum 1989).

First Generation PSs were based upon hematoporphyrin (Hp), an endogenous porphyrin, and its derivative (HpD). The first approved PS in the medical treatment of cancer was Photofrin in Canada (1993) for the treatment of bladder cancer. Since then, over 120 countries, including Portugal, approved the use of Photofrin for the treatment of different maladies as superficial bladder cancer, non-small cell lung cancer, esophageal carcinoma, gastric, cervical and endobronchial cancers (O'Connor et al. 2009). Although clinically approved, first generation PSs possess a huge setback as they induce high photosensitivity in the patient that could last weeks after treatment. Other disadvantages can be pointed as the non-selective accumulation in the target cells due to low specificity and the low penetration rate of only 5 mm due to the longest-

wave absorption band with low extinction coefficient (630 nm), allowing only the treatment of the most superficial diseases (Meyer-Betz 1913; O'Connor et al. 2009). To date, Photofrin is considered the gold standard for PDT.

Second Generation PSs appeared to overcome these disadvantages. PSs with new and improved properties were developed based on Photofrin. As examples of second generation PSs are benzoporphyrin derivates, chlorins, phthalocyanines, texaphyrins and naturally occurring compounds as hypericin and protoporphyrin IX. These compounds present an increased tissue penetration compared to first generation PSs, with strong absorbance in the red and near-infrared regions (600-800 nm) opposed to first generation allowing the treatment of deeper tumors. Although the improvements in comparison to first generation, these second generation PSs still possess a disadvantage as they do not present a localized distribution in the target area and have low selectivity to tumorous cells (Castano et al. 2004; O'Connor et al. 2009).

In order to oppose the setbacks of previous generations, researches started to study new forms of delivering and increase selectivity using first and second generation PSs. Using these prior generations and introducing or conjugating them with biochemical devices that would provide them improved target specificity, third generation PSs appeared with the most promising results to date. Many approaches have been used by researchers in order to increase PSs specificity to cancer cells. Although delivering systems, such as liposomes and nanoparticles, can improve their accumulation in tumors, both biomolecules with specificity for proteins overexpressed in tumors cells or conjugation of monoclonal antibodies directed against tumor antigens, have been shown promising results (Bugaj 2011).

Galactose-binding proteins (*i.e.* galectin-1 and galectin-3) and glucose transporters (*i.e.* GLUT1) are overexpressed in several types of cancers. The conjugation of sugars such as galactose, mannose or glucose to a porphyrinoid is then a valuable way to enhance the selectivity of the PS to tumour tissues (David 2010). Furthermore, the conjugation of carbohydrate targeting moieties gives the possibility of tuning the PS macrocycle amphiphilicity (Wojtyk et al. 2006).

1.2.2 Cell Death in PDT

The photodamage induced by PDT is a result of direct cytotoxic effects (Buytaert et al. 2008), vascular damage (Chen et al. 2002) and the induction of an immunity response (Garg et al. 2010).

Although PDT can mediate several cell signalling events, its ultimate purpose is to induce cell death. The mechanisms that mediate cell death after PDT have long been the subject of various studies. The mode and extent of cell death are influenced by several factors, including the concentration, physicochemical properties and subcellular localization of the PS, oxygen concentration, the intensity of light irradiation and cell type (Pereira et al. 2015)

When PS is activated with light at specific wavelengths photochemical reactions can lead to ROS production and cell damage by oxidizing and degrading cell components (Pereira et al. 2015). If cell repair mechanisms fail, damaged cells can then activate death signalling pathways. Under PDT, cells can undergo death by apoptosis, necrosis or autophagy (Silva et al. 2010; Gomer et al. 1988; Agarwal et al. 1993; Oleinick & Evans 1998; Separovic et al. 2011).

ROS produced after PDT have a short lifetime, acting in the vicinity to their site of generation. Therefore, subcellular localization of the PS determines the target of the primary damage. Subcellular locations of PS-induced ROS can be diverse, being the most described the endoplasmic reticulum, the mitochondria, lysosomes, plasmatic membrane, Golgi apparatus and PS binding directly to Bcl-2. The intrinsic web of events triggered after PDT, directly or indirectly, induces various changes in the cell signalling that can induce cell death. The main mechanisms involved in PDT efficiency are (1) the increase of the level of intracellular calcium; (2) phospholipases activation that lead to cell apoptosis; (3) the decrease of signal transduction of cell survival and cancer proliferation receptors; (4) activation of genes associated to apoptosis; (5) inducing over or under-expression of cytokines associated to inflammation and haematopoiesis; (6) inducing hypoxia through the consumption of molecular oxygen leading to stagnation of oxygen in the tumor region; (7) induction of stress related proteins and (8) alterations in cellular adhesion proteins (Robertson et al. 2009). The changes in cellular adhesion proteins are one of the most important consequences of PDT, as these changes will strongly affect cell behaviour, shape and the adhesion of tumor cells between themselves and to the substratum. Cell adhesion to the substratum is mediated by integrins and other cellular adhesion molecules that connect the extracellular matrix to the intracellular actin cytoskeleton (Tanaka et al. 2011). In that way, it is of interest to understand how the cytoskeleton is affected by PDT. In cancer metastasis, cell migration and invasion play a decisive role involving dissolution of the cellular matrix surrounding the cells, attachment of leading edge, detachment of the adhesions at the trailing edge of the cell, and cell contraction by myosin motifs inserting between F-actin filament bundles (Ridley 2003). These motility of the cells, only available thanks to the action of cytoskeletal structures that suffer continuous polymerization and depolymerisation, makes it one of the targets of interest in

photodynamic survival studies and in order to understand how inducing changes in this seemingly vital structures will affect the treatment outcome.

1.2.3 Changes in cytoskeleton induced by PDT

The three major cytoskeleton components presently known to be affected by PDT are microtubules (tubulin), intermediate filaments (vimentin) and actin filaments, being the later the one that shows more PDT-induced alterations across different cancer types and PSs and alterations in these components have been associated to tumor progression and metastasis (Vonarx et al. 1995). Due to the highly reported and spread alteration in actin filaments after PDT it is believed they play a central role in the early stage effects of phototherapy that eventually lead to cell death (Venosa 2015). These alterations are usually accompanied by changes in cell shape and morphology. But as previous described, the effects and activation of specific molecular pathways induced by PDT are highly dependent on several factors, such as cell type, fluence rate and specific PS (Venosa 2015).

Actin filaments are the structures most reported to be altered in response to PDT. The most reported alterations reported are changes in stress fibers, but with many conflicting results. Although some report increasing, others report a reduction of stress fibers after PDT. Another common effect is the redistribution of actin across the cell. But, as previously referred, for different cell lines and PSs, the effects observed greatly vary. Disorganization of original conformation of actin filaments seems to be one of the few common factors as loss of actin filaments (Tanaka et al. 2011; Lee et al. 1995; Uzdensky et al. 2005; Casas et al. 2008).

Microtubules are one of the structures that maintain cellular integrity and are involved in several homeostasis related processes but mainly in the establishment and maintenance of cell morphology. Microtubules are composed by two main types of tubulin, α and β, that combine to form dimeric structures that form the microtubule. Microtubule alterations after PDT have been previously reported. As a specific response to a PS, while vimentin intermediate filaments and actin stress fiber remained unaltered, it was reported that endoplasmic reticulum motility was inhibited as a result of the disruption of microtubules (Lee et al. 1995). Other studies suggest that the disruption of microtubules may stimulate the formation of stress fibers and the assembly of adhesion plaques. Other studies reported that in response to 5-aminolevulinic acid (ALA) PDT in two different cancer cell lines, the microtubules behaviour was distinct, while in one cell line microtubules remained practically unchanged, the other responded by the retraction of some cells and forming extracellular blebs of tubulin (Uzdensky et al. 2005).

Intermediate filaments (IF) are constituted by a multitude of different fibrous proteins, mostly vimentin in cells with mesenchymal origin, possessing mainly a structural function and giving mechanical stability to animal cells. IF are one of the less studied structures affected by PDT. It is known that the main component of IF, the protein vimentin, is degraded as a response to various inducers of apoptosis. In a study where a caspase resistant vimentin was transfected into cells, a partial suppression and delay of apoptosis PDT-induced was reported, suggesting an increased resistance by impairment of caspase-3 translocation (Belichenko et al. 2001).

Although cytoskeleton alterations have been widely reported after PDT, these alterations are highly variable with different outcomes for different cell lines suggesting that a deeper analysis of the complicated web of changes in the cytoskeleton has to be performed. Cytoskeleton alterations are known to have a strong effect over the processes leading to cell death. However, these alterations are believed to be correlated not only with cancer metastasis and invasiveness, but also with the development of PDT resistance (Robertson et al. 2009; Almeida et al. 2004; Tanaka et al. 2011). Many studies have been performed not only in order to identify why and how these changes occur, but also what other factors are associated to these alterations and how do they influence the treatment outcome.

Besides cytoskeletal and adhesion proteins, many other factors have been reported to have an important role in alterations induced after PDT. One protein of interest is RhoA. Belonging to the RhoA GTPases family, it is known that it is involved with a multitude of cellular processes including, but not limited to, cell division, actin cytoskeleton regulation and induction of formation of stress fibers and focal adhesion points. However, there is scarce information concerning whether disorganization of actin stress fibers after PDT is correlated with changes in RhoA protein levels.

Chapter 2. Objectives

Bladder cancer is a common malignancy in the urinary tract that has a high recurrence rate. Although the management of bladder cancer has significantly improved in the past years, the treatments available are not totally effective. It is of utmost importance the development of novel and more effective approaches to treat bladder cancer.

PDT consists of three individually nontoxic components - photosensitizer, light and molecular oxygen. However, when together they initiate a photochemical reaction leading to the generation of ROS. Cytotoxicity and cell death via apoptosis, necrosis or autophagy can occur via ROS. Several reports in the literature have shown that cell death pathway induced by PDT depends, among other factors, on the PS and its intracellular localization. Third generation PS coupled to galactose sugar seem to be interesting for research purposes since cancer tissues exhibit overexpression of certain galactose-binding proteins (Thijssen et al. 2015; Yau et al. 2015) increasing their specificity/uptake in cancer cells and reducing the unwanted phototoxicity in the neighbouring healthy tissues.

PDT for bladder cancer remains largely investigational having limited clinical use. We have previously reported $PorGal_8$, a galactodendritic porphyrin, as a new a water soluble third generation PS, able to generate ROS after photoactivation (Fig. 3) (Silva et al. 2012). In fact, $PorGal_8$ exhibits very interesting features as a PS: good aqueous solubility, without formation of aggregates up to 19 µM; with characteristic absorption spectra of porphyrins, high photo stability; demonstrated positive interaction with human serum albumin and positive oxygen singlet generation, suggesting that $PorGal_8$ has high potential as a PDT agent.

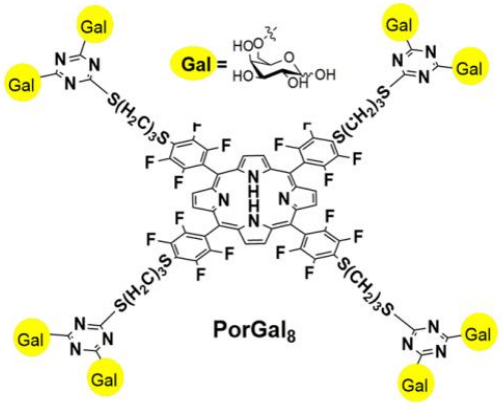

Figure 3. Schematic representation of $PorGal_8$, a porphyrin conjugated with four dimeric structures of galactose (Silva et al. 2012)

More recently, we have validated $PorGal_8$ as a novel therapeutic agent for the treatment of tumors containing high levels of galactose-binding proteins, namely galectin-1 (Pereira et al. 2016). We have shown a specific uptake of this PS and induction of ROS-mediated cell death. We have also validated the photodynamic efficiency of $PorGal_8$ in an immunodeficient animal model bearing subcutaneously implanted a bladder cancer xenograft, overexpressing galectin-1 protein.

Despite it is known that cell death mechanisms induced after PDT can instigate changes and reorganization on the main cytoskeletal components (microtubules, microfilaments and intermediate filaments), little is known about the underlying mechanisms.

The main goal of this work is to investigate whether the phototoxicity induced by $PorGal_8$ is correlated with alterations in cytoskeletal structures of cancer cells.

In order to accomplish this, we propose to:

- Evaluate cellular uptake and phototoxicity effects of the $PorGal_8$ in two bladder cancer cell lines, UM-UC-3 and HT-1376.

- Investigate changes in the levels and subcellular redistribution of cytoskeleton components - microtubules, microfilaments and intermediate filaments - after PDT with $PorGal_8$.

- Investigate the role of RhoA in cytoskeleton disorganization after $PorGal_8$-PDT.

Chapter 3. Materials and Methods

3.1 Preparation of $PorGal_8$ working solution

A porphyrin conjugated with dendritic units of galactose ($PorGal_8$) was synthesized and characterized in the "Porphyrins and Phthalocyanines Materials Research Group", Department of Chemistry, University of Aveiro, Portugal (Silva et al. 2012).

Stock solutions of the $PorGal_8$ at a concentration of 2 mM were prepared in dimethyl sulfoxide (DMSO, Sigma Ref. D2650). After solubilization at 35 kHz for approximately forty minutes in an ultrasonic bath (Sonorex, TK52, Bandelin), stock solutions were stored at 0-4 °C in dark conditions. Freshly working solutions were prepared from stock solution in sterile phosphate-buffered saline (PBS, 137 mM NaCl, 27 mM KCl, 81 mM Na_2HPO_4, 15 mM KH_2PO_4, pH 7.30), accounting their water solubility range. The concentration of DMSO was always lower than 0.5% (v/v), in the working solutions.

3.2 Cell Culture

The cell lines from transitional cell carcinoma of human urinary bladder were obtained from the American Type Culture Collection. UM-UC-3 (ATCC Number: CRL-1749^{TM}) cell line with epithelial-like characteristics was derived from a high grade invasive bladder carcinoma of a male patient. HT-1376 (ATCC Number: CRL-1472^{TM}) cell line was derived from a 58 years old caucasian female with a grade 3 carcinoma of the bladder.

UM-UC-3 and HT-1376 grown in monolayer were cultured in Roswell Park Memorial Institute (RPMI)-1640 medium (Sigma-Aldrich, Ref. R4130), supplemented with 2 g/L sodium bicarbonate (Sigma-Aldrich, Ref. S5761), 10% (v/v) heat-inactivated Fetal Bovine Serum (FBS; Gibco, Ref. 10270-106), 1% (v/v) antibiotic/antimycotic containing penicillin, streptomycin and amphotericin B (Sigma-Aldrich , Ref. 15240-062) and 2mM L-Glutamine (BioWest, Ref. X0550-100), at 37 °C in a humidified atmosphere with 5% CO_2 and 95% of air. Cells were subcultured one to three times a week when they reached approximately 80% of confluence. To check cell viability before plating the cells for the experiments, they were trypsinized and resuspended in medium. Then, a mixture of cell suspension and trypan blue stain (1:1) was prepared to count the cells on a Neubauer chamber. The percentage of viable cells and the concentration of viable cells per milliliter of cell suspension were calculated. Only cells with a viability above 90% were used in all experiments.

3.3 Determination of total protein concentration

The protein concentration in cell extracts was measured spectrophotometrically using the BCA assay kit (BCA/Smith Assay; Pierce, Ref. 23227) using bovine serum albumin as a standard in a 96-well cell culture plate (Orange Scientific). This procedure involves two steps: the first is the biuret reaction in an alkaline environment, whose faint blue colour results from the reduction of cupric ion (Cu^{2+}) to cuprous ion (Cu^{1+}) by peptide bonds in protein, therefore, the amount of reduced Cu^{2+} is proportional to the amount of protein present in the solution. The second step is the chelation of two molecules of BCA with one cuprous ion using the reagent containing bicinchoninic acid, resulting in a water-soluble complex product with intense purple colour that strongly absorbs light at the wavelength of 562 nm.

i) Determination of total protein concentration for cellular uptake of $PorGal_8$ assay (cells solubilized in 1% (m/v) SDS solution in PBS pH 7.0)

In a 96-wells plate, the following solutions were pipetted into each well: 25 µL of sample buffer (1% (m/v) SDS (sodium dodecyl sulphate, Biorad Ref. 161-0301-100g) in PBS (pH 7.0)); 25 µL of sample, blank (sample buffer), BSA standard (prepared in the sample buffer at concentrations ranging from 12.5 - 800 $\mu g.mL^{-1}$ prepared from the BSA standard at 2 $mg.mL^{-1}$); and 200 µL of BCA working Reagent (fifty parts of BCA reagent A mixed with one part of BCA reagent B).

ii) Determination of total protein concentration for Western blot analysis (cells solubilized in RIPA buffer)

In a 96-wells plate, the following solutions were pipetted to each well: 25 µL of sample buffer (RIPA buffer: 150 mM NaCl, 50 mM Tris base, 5 mM EGTA, 0.5% (m/v) DOC, 0.1% (m/v) SDS, 2 mM PMSF, 2 mM IAD, 1 tablet of protease inhibitor cocktail, pH 7.50); 25 µL of sample diluted in RIPA buffer 1:9 (v/v), blank (sample buffer), standard (prepared in the sample buffer at concentrations ranging from 12.5 - 800 $\mu g.mL^{-1}$ using the BSA standard at 2 $mg.mL^{-1}$); and 200 µL of BCA working Reagent (50 parts of BCA reagent A mixed with one part of BCA reagent B).

The plate was incubated at 37 °C for 30 min. Then, the absorbance at 570 nm was measured on a microplate reader Synergy™ HT (Biotek Instruments) controlled by BioTek's Gen5™ Data Analysis Software. The protein concentration in the samples was directly obtained by

plotting the average of the absorbance at 570 nm for each BSA standard in function of its concentration ($\mu g.mL^{-1}$) (Smith et al. 1985).

3.4 Preparation and treatment of cancer cells with $PorGal_8$

UM-UC-3 and HT-1376 cells were seeded at a density of approximately 9.4 x 10^4 $cells.cm^{-2}$ in culture plates (Orange Scientific). Twenty-four hours after plating, the culture medium was removed and the cells were washed once with sterile PBS. Cells were then incubated with $PorGal_8$ (in PBS containing < 0.5% (v/v) DMSO) in the dark for ninety minutes.

3.5 Cellular Uptake of $PorGal_8$

Based on the fluorescence properties of the porphyrin $PorGal_8$, its concentration inside the cancer cells can be determined by fluorimetry (after cell lysis) and normalized to total protein quantity.

For this assay, UM-UC-3 and HT-1376 cells were seeded at a density of 3 x 10^4 cells/well in a 96-well culture plates (Orange Scientific) as previously described. After incubation with the desired concentrations of $PorGal_8$ in the dark, cells were immediately washed with PBS buffer at pH 7.0 and lysed in 120 µL of 1% (m/v) sodium SDS solution in PBS (pH 7.0) with gentle continuous agitation on an automatic plate shaker in the dark for 30 min at RT. Ninety µL of this cell suspension was transferred to 96-wells black plates and the intracellular fluorescence of $PorGal_8$ was determined by fluorometric measurement in an microplate reader Synergy™ HT (Biotek Instruments), using standard $PorGal_8$ solutions for construction of a calibration curve. Fluorescence readings used the excitation and emission filters set at 360/40 nm and 645/40 nm, respectively. $PorGal_8$ concentration in the samples was directly obtained by comparison to the standard curve and the results were normalized for protein concentration (determined by the BCA/Smith assay as previously described).

3.6 Photodynamic assay

After $PorGal_8$ incubation, the cells were washed once with PBS and covered with fresh RPMI-1640 medium. In a dark room, the cells were irradiated for forty minutes with a LEDs array system emitting white light with two emission peaks at $\lambda = 450 \pm 20$ and $\lambda = 550 \pm 50$ nm. The cell culture plates were placed above the LEDs (Fig.4) Under these conditions, most of the light was emitted at a potency of 8.4 $mW.cm^{-2}$. After irradiation, cells were either immediately used for the determination of cell uptake of $PorGal_8$ assay or washed once with PBS and incubated with RPMI-

1640 medium for selected time points (thirty minutes or twenty-four hours depending of the assay) in the humidified incubator gassed with 5% CO_2 and 95% air.

The Dark assays were similarly handled to the PDT assay, being kept in the dark in the incubator for the forty minutes corresponding to the irradiation treatment.

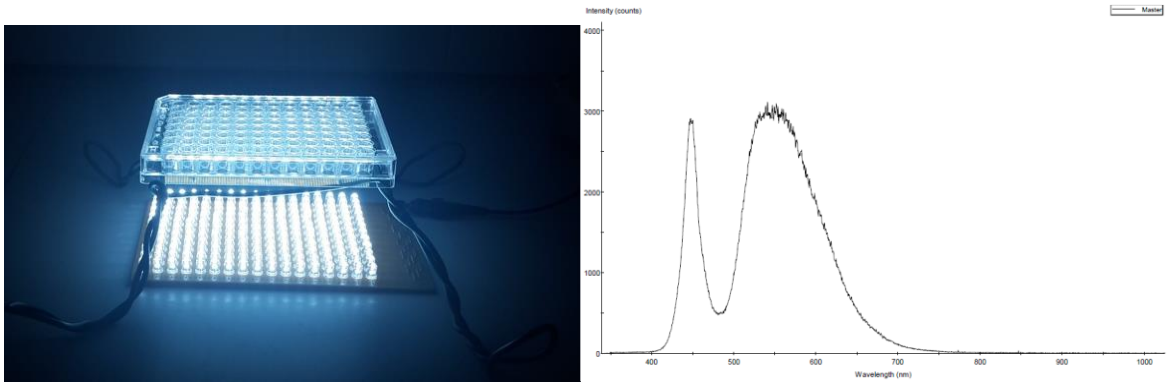

Figure 4. (Left) Representative image of LED array system and (Right) Emission spectra of the LED array system used in the irradiation assays. Composed of a matrix of 24 x 16 LEDs totalizing 384 light sources emitting white light with two emission peaks at λ = 450 ± 20 and λ = 550 ±50 nm. The used regulated Plug-in adaptor with LED indicator 800 mA was purchased from MW.

3.7 Cell viability assays

The evaluation of the cytotoxicity effects of the $PorGal_8$ was evaluated twenty-four hours after incubation with $PorGal_8$ and treatment (dark or irradiated) as previously described. For this evaluation two assays were performed: MTT (3-[4,5-dimethylthiazol-2-yl]-2,5-diphenyl-tetrazolium bromide) colorimetric and Trypan Blue assays.

i) MTT colorimetric assay

For this assay UM-UC-3 and HT-1376 cells were seeded at a density of 3.0 x 10^4 cells/well in a 96-well culture plates, as previously described. Cell metabolic activity after treatment (dark or irradiated), was determined 24 h after treatments by measuring the ability of bladder cancer cells to reduce MTT (yellow coloured, Sigma, Ref. M2128-1G) to an insoluble formazan product (with a blue purple colour), being this reduction proportional to the mitochondrial enzyme succinate dehydrogenase activity. Briefly, twenty four hours after treatment, 50 µL of medium was removed and 10 µL of MTT stock solution (3 $mg.mL^{-1}$ in PBS buffer) was added to each well at a final concentration of 0.5 $mg.mL^{-1}$. The plates were then incubated in the darkness at 37 °C for 2 hours. The resulting purple needle-shaped crystals were dissolved by the addition of 150 µL acidic isopropanol (0.04 M HCl in absolute isopropanol). To solubilize completely the converted dye, repetitive pipetting was applied. The absorbance was measured at 570 nm (using 620 nm as the

background wavelength), using a microplate reader (Synergy HT, Biotek). The data were expressed in percentage of control (untreated cells) (Mosmann 1983).

For each well, the absorbance was expressed as:

$$Absorvance\ 570\ nm - Absorvance\ 620\ nm$$

The results were expressed as percentage of MTT reduction:

$$MTT\ reduction\ (\%) = \frac{Absorvance\ treated\ wells}{Absorvance\ control\ wells} \times 100\%$$

ii) Trypan Blue dye exclusion

The UM-UC-3 and HT-1376 cells were plated at a density of 8.9 x 10^4 cells/ well (250 µL), in 48-wells culture plates, as previously described. Cell membrane integrity after $PorGal_8$ incubation, was determined 24 h after treatment (dark or irradiated) by trypan blue dye exclusion assay. Once trypsinized, an aliquot of the cellular suspension was diluted in the trypan blue stain (1:1) and the cells were counted for determination of both viable and nonviable cells. The organic amine dye trypan blue would be excluded from viable (living) cells with intact membrane appearing bright under the microscope while nonviable cells (cells with compromised membrane integrity) would appear stained in blue.

Viable (bright cells) and nonviable cells (cells stained in blue) were counted and summed for the total number of cells. The viability was calculated as follows:

$$Viable\ cells\ (\%) = \frac{Number\ of\ Viable\ Cells}{Number\ of\ Total\ Cells} \times 100\ \%$$

The concentration of viable cells per millilitre in the cell suspension was calculated considering the average of viable cells per each counting square, the dilution made and the volume of each counting square: $\frac{Viable\ Cells}{mL} = \frac{VCs \times dilution\ factor}{1 \times 10^{-4}}$

3.8 Preparation of Cellular Extracts of UM-UC-3 and HT-1376 cells for Western Blotting

For immunodetection of proteins, UM-UC-3 and HT-1376 cells were plated at a density of 8.93 x 10^5 cells/well (1.5 mL per well), in a 6-well culture plate for 24 h before treatment. The cells were then treated with 10 µM $PorGal_8$ (500 µL) and the photodynamic treatment was performed as previously described. After treatment, cells were washed once with PBS (500 µL) and incubated in RPMI-1640 medium for thirty minutes or twenty-four hours in the humidified incubator gassed with 5% CO_2 and 95% air. UM-UC-3 and HT-1376 cells were washed once with ice-cold PBS (500

µL) and then with ice-cold OVNA 0.5 mM (500 µL; sodium orthovanadate in PBS Buffer, Sigma S6508) and lysed with ice-cold RIPA (200 µL; buffer with fresh protease inhibitors). The cell lysates were then transferred to microtubes with the help of a rubber policeman (cell scrapper) and incubated on ice during 30 min. During incubation, samples were vortexed 10 seconds every 5 minutes. The total cell lysates were centrifuged at 18,000 *x g* for 16 minutes, at 4 °C. The supernatant was transferred to a new microcentrifuge tube. The supernatants were used for protein concentration determination (Smith/BCA Assay) as previously described, followed by denaturation with Laemmli buffer 6x (350 mM Tris-HCl, pH 6.8, 30% (m/v) glycerol, 10% (m/v) SDS, 600 mM DTT, 0.012% (m/v) bromophenol blue, pH 6.80). Cellular extracts were stored at -20 °C after denaturation (Laemmli 1970).

3.9 Western Blotting

3.9.1 Sodium Dodecyl Sulphate Polyacrylamide Gel Electrophoresis and Blotting

The samples were heated at 37 °C for 30 minutes. Thirty to forty µg of protein samples were loaded on polyacrylamide gels and the proteins were separated by electrophoresis. The electrophoresis was stopped when the dye front reached the bottom of the gel. Following gel electrophoresis, the separated protein mixtures were transferred to a solid support for further analysis. The polyvinylidene difluoride membranes (Immun-Blot PVDF membranes, BioRad) were first activated with 100% MetOH, and then soaked in Milli-Q water and equilibrated in transfer buffer. All the material used in the blotting (sponges, sheets of filter paper), as well as the gels were also equilibrated in transfer buffer. The gel and the PVDF membrane were assembled into a sandwich along with sheets of filter paper and sponges. The separated proteins were then transferred to the PVDF membranes (using ice cold transfer buffer) for 90 min under agitation, the tank in ice (and using a cooling coil inside the tank). At the end, the baking of the membranes was performed by incubation at 50 °C for 20 min (Towbin et al. 1979).

Table 1. Primary Antibodies used in western blotting (WB) and immunocytochemistry (ICC) assays

Antibody	Dilution		Supplier	Ref.
	WB	ICC		
Mouse anti β-actin	1 : 20000	---	Sigma-Aldrich	A5441
Mouse anti Vimentin Ab-2	1 : 1000	1 : 250	ThermoFisher	MS-129-P1
Mouse anti α-Tubulin	1 : 1000	1 : 500	Sigma-Aldrich	T6199
Rabbit anti RhoA	1 : 5000	1 : 300	Abcam	ab187027

3.9.2 Antibodies incubations, detection and quantification

The membranes were placed into blocking buffer (5% (v/v) non-fat milk or 3% (v/v) BSA, prepared in tris buffer saline tween20 (TBST buffer; 20 mM Tris base, 150 mM NaCl, 0.1% (v/v) Tween 20, pH 7.60) for thirty to ninety minutes at RT with gentle agitation. The membranes were incubated with the primary antibody, diluted in 2.5% non-fat milk, prepared in TBST), for two hours at RT, under low agitation. After incubation, the membranes were rinsed in TBST (3 x 10 min) at RT. The appropriate secondary antibody conjugated with the enzyme horseradish-peroxidase diluted 1:10,000 (v/v) in 2.5% non-fat milk (prepared in TBST) was added, and the membranes were incubated for one hour at RT, under moderate agitation. After incubation with the secondary antibodies, the membranes were washed in TBST (3 x10 min), with agitation. To demonstrate equivalent protein loading, all the membranes were re-probed for the protein β-actin. For the detection, the membranes were placed on the chemiluminescence detection system Chemi Doc™ XRS (Bio-Rad) controlled by the software Quantity One (proteins side up), incubated with the substrate solution (1:1, by volume, mixture of luminol/enhancer and peroxide buffer; Immun-Star™ WesternC™ Chemiluminescent Kit, BioRad) for 1 min following manufacturer instructions, and then the images were acquired. The intensity signal of the bands was quantified using the software ImageJ 1.6 and the fold change in protein levels were expressed as follows and then normalized to the control situation:

$$Fold\ change\ in\ protein\ expression\ = \frac{Protein\ Band\ Density}{\beta - Actin\ Band\ Density}$$

3.10 Immunofluorescence assays and Confocal Microscopy

For visualization of the distribution of specific proteins associated to cytoskeleton structures (for microtubules tubulin and for intermediate filaments vimentin) and cell death (RhoA) through the sample immunocytochemistry assays were performed. For the visualization of F-actin filaments staining using Phalloidin–Tetramethylrhodamine B isothiocyanate (TRITC-conjugated phalloidin; Sigma, Ref. P1951) was performed (Casas et al. 2008).

One coverslip/well (Warner Instruments) in 24-wells culture plates were coated with poly-L-lysine (Sigma, Ref. P4707) (80 µL) for 30 to 40 minutes at RT. The poly-L-lysine was removed and the coverslips were allowed to completely dry for 30 minutes at RT. The UM-UC-3 and HT-1376 cells were plated carefully at a density of 1.75 x 10^5 cells/well (500 µL) for 24 h before treatment. After $PorGal_8$ incubation and treatment as previously described the plates were incubated for thirty minutes to twenty-four hours after treatment, dark or irradiated. After the incubation periods, cells were washed once with PBS.

i) Immunocytochemistry Assays (for tubulin, vimentin and rhoA antibodies)

After washing with PBS, cells were fixed with the appropriate fixator (300 µl) and time according to the target protein structure and cell line. For immunostaining with tubulin for both UM-UC-3 and HT-1376 cell lines, and vimentin for UM-UC-3 cells, fixation was performed with ice-cold MES buffer (100mM 2-(N-morphilino)-ethane sulphonic acid, 1 mM EGTA, 1mM $MgSO_4$, 90% MetOH (v/v), pH 6.90) during five minutes; HT-1376 cells destined to be immunostained with vimentin were fixed with ice-cold MetOH during five minutes; when destined to immunostaining with RhoA antibody both cell lines were fixed with PFA 4% (prepared in PBS buffer, pH 7.30) during ten minutes. The samples were after fixation washed with PBS (3 x 5 min). The cells were treated with permeabilization buffer (1% (v/v) Triton X-100, 0.02% (m/v) BSA, 0.02% (m/v) NaN_3, prepared in PBS, pH 7.30) (250 µl) during 10 min. Cells were then washed with washing buffer ((0.02% (m/v) BSA (VWR, Ref. 441554Y), 0.02% (m/v) NaN_3, Prepared in PBS, pH 7.30), three times each five minutes. The cells were then incubated with the blocking buffer (5% (v/v) BSA, prepared in PBS buffer) for 20 min, in a humidified chamber. After blocking, the cells were incubated with the primary antibody diluted in washing buffer during ninety minutes at RT, in a humidified chamber in the dark. The primary antibody solution was decanted and the samples were washed with washing buffer (3 x 5 min). The cells were incubated with the secondary antibody and 4',6-Diamidino-2-phenylindole (DAPI, Enzo Life Sciences) (1 $\mu g.mL^{-1}$) diluted in washing buffer for sixty minutes at RT, in a humidified chamber in the dark. The secondary anti-rabbit or anti-mouse antibodies used were the Alexa Fluor 488 Goat Anti-Rabbit and Alexa Fluor 568 Goat Anti-Mouse (Molecular Probes). The cells were washed again with the washing buffer (3 x 5 min). The coverslips were mounted using the glycergel mounting medium and sealed with nail polish. The samples were stored in an appropriate box at 4 °C until acquisition of images by fluorescence microscopy (confocal microscope from Zeiss; LSM 710, Carl Zeiss).

ii) F-Actin Staining

After washing with PBS, cells were fixed with 4% PFA (300 µl) for 30 min at RT. Samples were washed with PBS (3 x 5 min), dehydrated with acetone then permebealized with 0.1% Triton X-100 (prepared in PBS, 250 µl) and washed again with PBS (3 x 5 min). To visualize actin filaments samples were incubated with 50 $\mu g.mL^{-1}$ TRICT-conjugated phalloidin and DAPI (1 $\mu g.mL^{-1}$) diluted in PBS buffer for forty minutes. The samples were again washed with PBS (3 x 5 min). The coverslips were mounted using glicergel mounting medium and stored at 4 °C until visualization under the fluorescence microscope.

Chapter 4. Results

4.1 PorGal$_8$ accumulates in bladder cancer cells

Our group previously reported PorGal$_8$, a porphyrin conjugated with dendritic units of galactose, as a new and efficient third generation PS for PDT against two bladder cancer cell lines, HT-376 and UM-UC-3, which were derived from transitional cell carcinoma (Silva et al. 2012; Pereira et al. 2016). The present study was undertaken to investigate whether phototoxicity induced by PorGal$_8$ is correlated with alterations in skeletal structures of cancer cells.

We started to determine the concentration of PorGal$_8$ inside the UM-UC-3 and HT-1376 cells by spectrofluorimetry, in order to determine the optimum concentration to be used in the following assays. Bladder cancer cells were incubated with increasing concentrations (0.5, 2.5, 5, 10 and 12.5 μM) of PorGal$_8$ in PBS for ninety minutes in the dark. The intracellular concentration of PorGal$_8$ was determined using a calibration curve using known concentrations of the PS (Fig. 5).

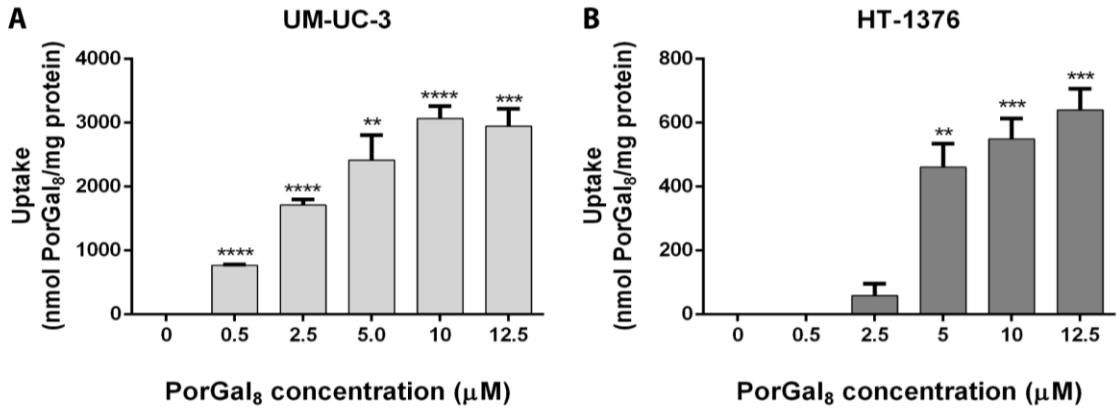

Figure 5. Intracellular uptake of PorGal$_8$ by UM-UC-3 (A) and HT-1376 (B) bladder cancer cells. Cells were incubated in the darkness with increasing concentration of PorGal$_8$ (0.5, 2.5, 5, 10 and 12.5 μM) for ninety minutes. The concentration of PorGal$_8$ was determined by fluorescence spectroscopy and the results were normalized to total protein quantity. Data are the mean value ± S.E.M. (standard error of mean) of at least three independent experiments performed in triplicates. **($p<0.01$), ***($p<0.001$), **** ($p<0.0001$) significantly different from control cells (incubated with PBS).

The cellular uptake of PorGal$_8$ was concentration-dependent and higher in UM-UC-3 than HT-1376 cells. Maximum intracellular accumulation of PorGal$_8$ was achieved when cells were incubated between 10 -12.5 μM of the PS. UM-UC-3 and HT-1376 cells incubated for ninety minutes with 10 μM PorGal$_8$, presented an intracellular concentration of 3068 ± 333 and 549 ± 109.9 nmol PorGal$_8$ per mg of protein, respectively (Fig. 5A and B).

4.2 $PorGal_8$ induces phototoxicity in bladder cancer cells

After confirmation of $PorGal_8$ uptake by bladder cancer cell lines, its cytotoxicity in the dark was assessed 24 h after treatment by MTT and Trypan Blue assays. No dark toxicity was observed in untreated cells (up to ninety minutes) in the presence of 0.5% DMSO in PBS. In both cell lines, incubation with 10 µM $PorGal_8$ in the dark did not induce toxicity (Fig. 6A, B, C and D). To test the effect of light irradiation (white light LED system, delivered at 8.4 $mW.cm^{-2}$ for forty min) immediately after $PorGal_8$ uptake, cell viability assays were also performed 24 h after treatment. White irradiation of cells (previously incubated with PBS containing 0.5% DMSO for ninety min in the dark) *per se* did not induce toxicity (data not shown). However, when both cell lines were incubated with 10 µM $PorGal_8$ and then irradiated, there was an increased phototoxicity.

When cells were incubated with 10 µM $PorGal_8$ for ninety min and then irradiated, a significant decrease in cell viability was observed. The phototoxicity was higher in UM-UC-3 cells than in HT-1376 cells. Photoactivation of 10 µM $PorGal_8$ induced a decrease in MTT reduction, from 100% to 53.62 ± 5.93 ($p<0.001$) in UM-UC-3 cells and to 80.33 ± 8.26 ($p<0.05$) in HT-1376 cells (Fig. 6A and C). Trypan blue exclusion assay was used to confirm viability results obtained by MTT. Photoactivation of 10 µM $PorGal_8$ induced a decrease in the percentage of excluded dye, from 100% to 57.07 ± 9.25 ($p<0.0001$) in UM-UC-3 cells and to 76.84 ± 4.68 ($p<0.0001$) in HT-1376 cells (Fig. 6B and D).

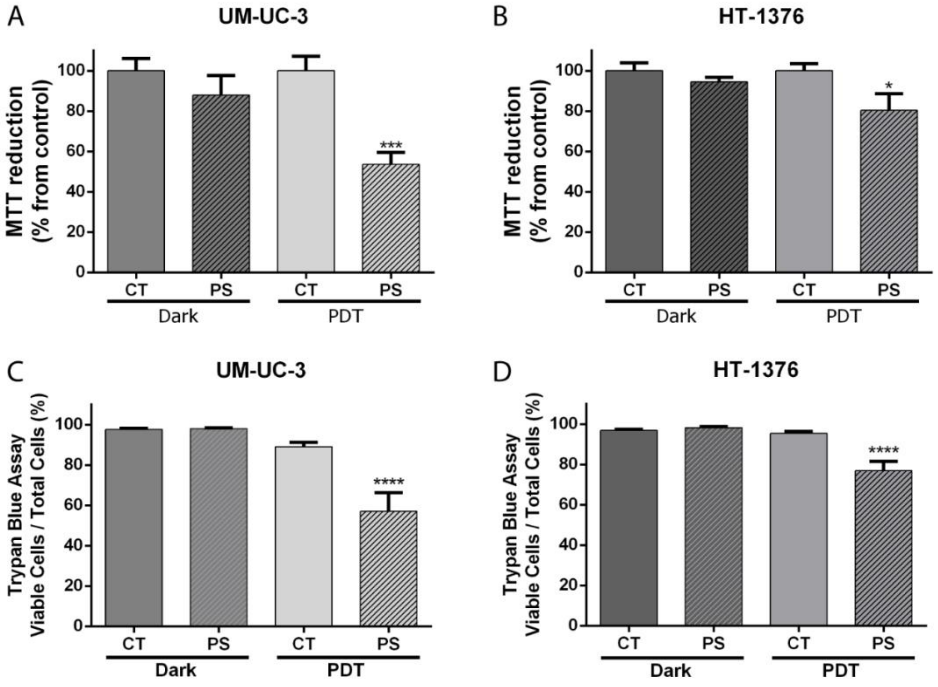

Figure 6. $PorGal_8$ is nontoxic in darkness and induces toxicity after its photoactivation in UM-UC-3 (A, B) and HT-1376 (C, D) cells. Cells were incubated with 10 µM $PorGal_8$ incubation in dark

conditions for ninety min. Cell viability was evaluated 24 hours after treatment (dark or after irradiation with 8.4 $mW.cm^{-2}$ for 40 min) using the MTT colorimetric (A, C) and Trypan Blue assays (B, D) in UM-UC-3 and HT-1376 cell lines. The percentage of toxicity was calculated relatively to control cells (cells incubated with PBS). MTT reduction data (A and C) is presented as the mean ± S.E.M of at least two independent experiments (dark conditions) and four independent experiments (after irradiation) performed in triplicates. Not significantly different from control cells in dark assays. *($p<0.05$), ***($p<0.001$) significantly different from control cells. For trypan blue assays data (B and D) is presented as the mean ± S.E.M. of one independent experiment in sextuplicates (dark treatment) and three independent experiments in triplicates (irradiation treatment). *($p<0.05$), **** ($p<0.0001$) significantly different from control cells.

4.3 Cytoskeleton disorganization after PDT with $PorGal_8$

To evaluate whether cell death induced by PDT with $PorGal_8$ is associated with changes in cytoskeleton, its three major components – microtubules, microfilaments and intermediate filaments - were evaluated 30 min or 24 h after treatment, by Western Blotting and/or fluorescence microscopy.

$PorGal_8$ did not induce any significant changes in the protein levels of α-tubulin, which is one of the main constituents of the microtubules, 30 min or 24 h after PDT in UM-UC-3 (Fig. 7).

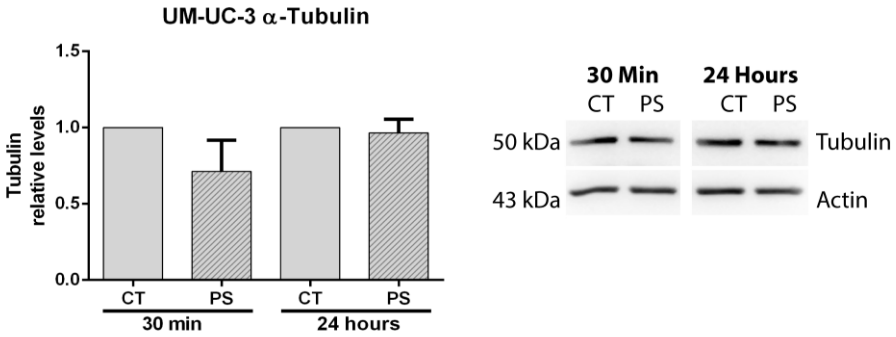

Figure 7. $PorGal_8$ does not induce changes in α-tubulin protein levels after photodynamic activation in UM-UC-3 cells. Western blot analysis and quantification of α-tubulin protein levels in UM-UC-3 cells 30 min and 24 h after irradiation. β-actin was blotted as loading control. Quantitative analysis of α-tubulin (normalized to β-actin) expressed as ratio to controls (cells incubated with PBS instead of $PorGal_8$) in UM-UC-3 cell line. Data represents the mean ± S.E.M. of at least four independent experiments.

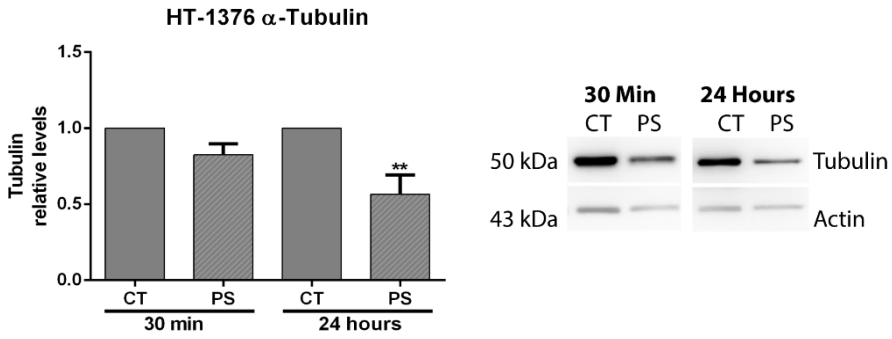

Figure 8. PorGal$_8$ reduces α-tubulin protein levels after photodynamic activation in HT-1376 cells. Western blot analysis and quantification of α-tubulin protein levels in HT-1376 cells 30 min and 24 h after irradiation. β-actin was blotted as loading control. Quantitative analysis of α-tubulin (normalized to β-actin) expressed as ratio to controls (cells incubated with PBS instead of PorGal$_8$) in the HT-1376 cell line. Data represents the mean ± S.E.M. of at least four independent experiments. **($p<0.01$) significantly different 24 h after PorGal$_8$-PDT from control cells in HT-1376 cell line.

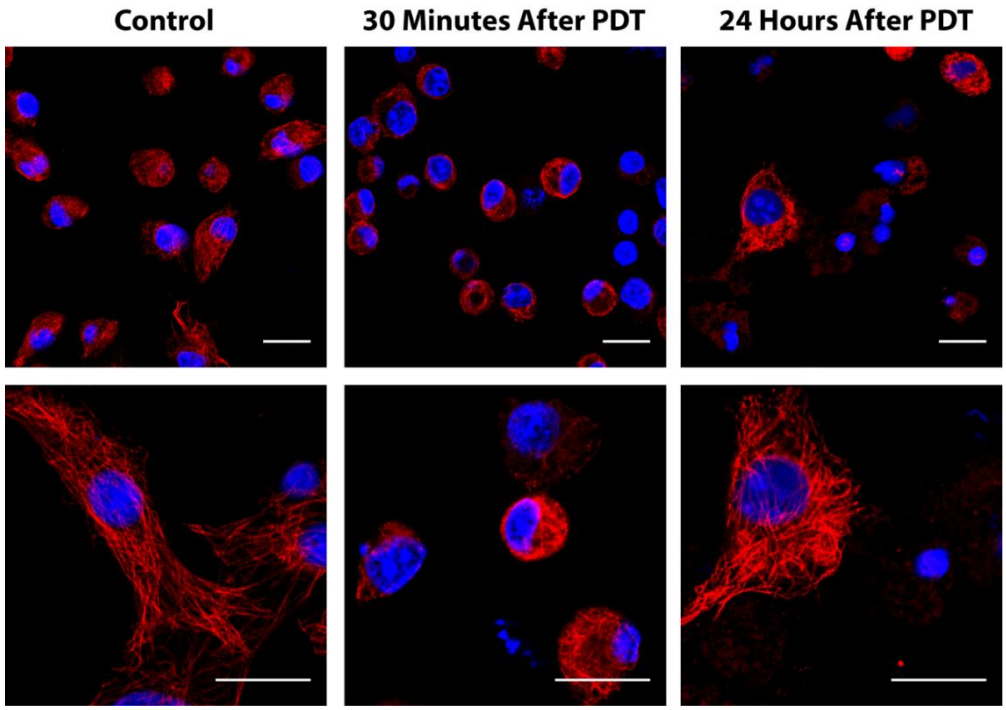

Figure 9. Changes of α-tubulin in HT-1376 cells 30 min and 24 h after targeted PDT with PorGal$_8$. Immunofluorescence detection of α-tubulin (red). The nuclei were stained with DAPI (blue). Scale bars 20 μm.

Although no significant changes in the protein levels of α-tubulin 30 min after treatment were detected, a significant decrease in α-tubulin protein content was observed 24 h after PDT in HT-1376 cells (Fig. 8). Control HT-1376 cells presented well-organized microtubule networks within cell´s cytoplasm. In contrast, PDT-treated HT-1376 cells displayed a rearrangement of

microtubule networks to a round shape and disorganized microtubules 30 min after irradiation. After 24 h, although a few cells showed a recovery in microtubules organization, the fluorescence intensity decreased noticeably in most of the cells (Fig. 9).

$PorGal_8$ did not induce any significant changes in the protein levels of vimentin in UM-UC-3 and HT-1376 cells 30 min after PDT. However, 24 hours after irradiation both cell lines presented a reduction in the protein levels of vimentin (Figs. 10 and 11).

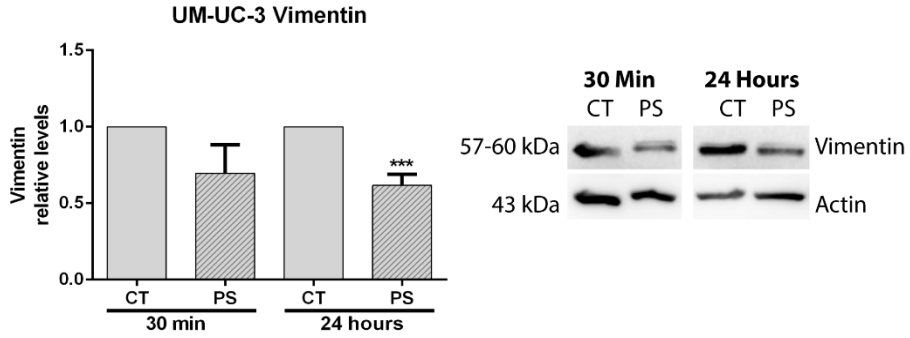

Figure 10. $PorGal_8$ induces changes in vimentin protein levels after photodynamic activation in UM-UC-3 cells. Western blot analysis and quantification of vimentin protein levels in UM-UC-3 cells 30 min and 24 h after irradiation. β-actin was blotted as loading control. Quantitative analysis of vimentin (normalized to β-actin) expressed as ratio to controls (cells incubated with PBS instead of $PorGal_8$) in UM-UC-3 cell line. Data represents the mean ± S.E.M. of at least three independent experiments. ***($p<0.001$) significantly different from control cells in UM-UC-3 cell line twenty-four hours after $PorGal_8$-irradiation.

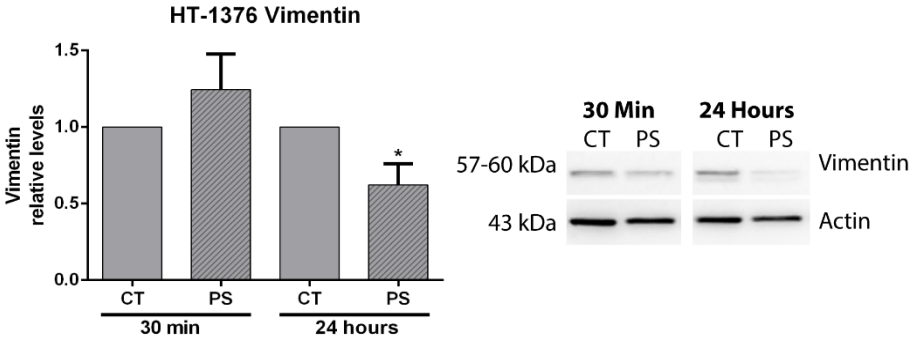

Figure 11. $PorGal_8$ reduces vimentin protein levels after photodynamic activation in HT-1376 cells. Western blot analysis and quantification of vimentin protein levels in HT-1376 cells 30 min and 24 h after irradiation. β-actin was blotted as loading control. Quantitative analysis of vimentin (normalized to β-actin) expressed as ratio to controls (cells incubated with PBS instead of $PorGal_8$) in the HT-1376 cell line. Data represents the mean ± S.E.M. of at least five independent experiments. *($p<0.05$) significantly different from control cells in HT-1376 cell line twenty-four hours after irradiation-$PorGal_8$.

In control HT-1376 cells vimentin labelling revealed a filamentous network in the cytoplasm, which extends towards the cell edge. Thirty minutes after irradiation, the vimentin also appeared as a filamentous network in the cytoplasm, that was near to the plasma membrane but rarely extended to it. Twenty-four hours after irradiation, most of the cells staining is reduced (Fig. 12)

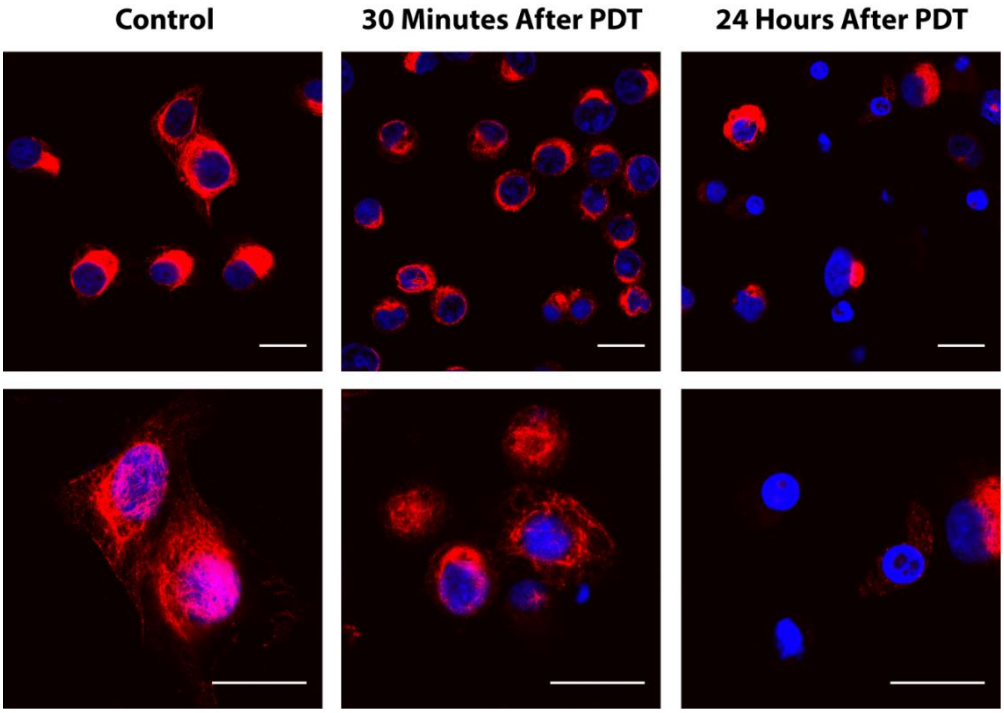

Figure 12. Changes of vimentin in HT-1376 cells 30 min and 24 h after targeted PDT with PorGal$_8$. Immunofluorescence detection of vimentin (red). The nuclei were stained with DAPI (blue). Scale bars 20 μm.

Staining with Phalloidin-TRITC (for detection of F-actin) in both UM-UC-3 and HT-1376 control cells showed the presence of long stress fibres (Fig. 13 and 14). Thirty minutes after irradiation, UM-UC-3 cells were rounded and showed a retraction of actin filaments with loss of stress fibres**.** Twenty-four hours after treatment, some features of actin disorganization remained present, no stress fibres were observed and phalloidin fluorescence was stronger in locations of cell-to-cell contact (Fig. 13).

After thirty minutes, similar to what observed to UM-UC-3 cells, HT-1376 cells showed a clear retraction of actin filaments with loss of stress fibers**.** However, twenty-four hours after treatment, some cells present some reorganization in actin filaments, presenting short stress fibers, long extensions, like large filopodia, which suggests a possible recovery (Fig. 14).

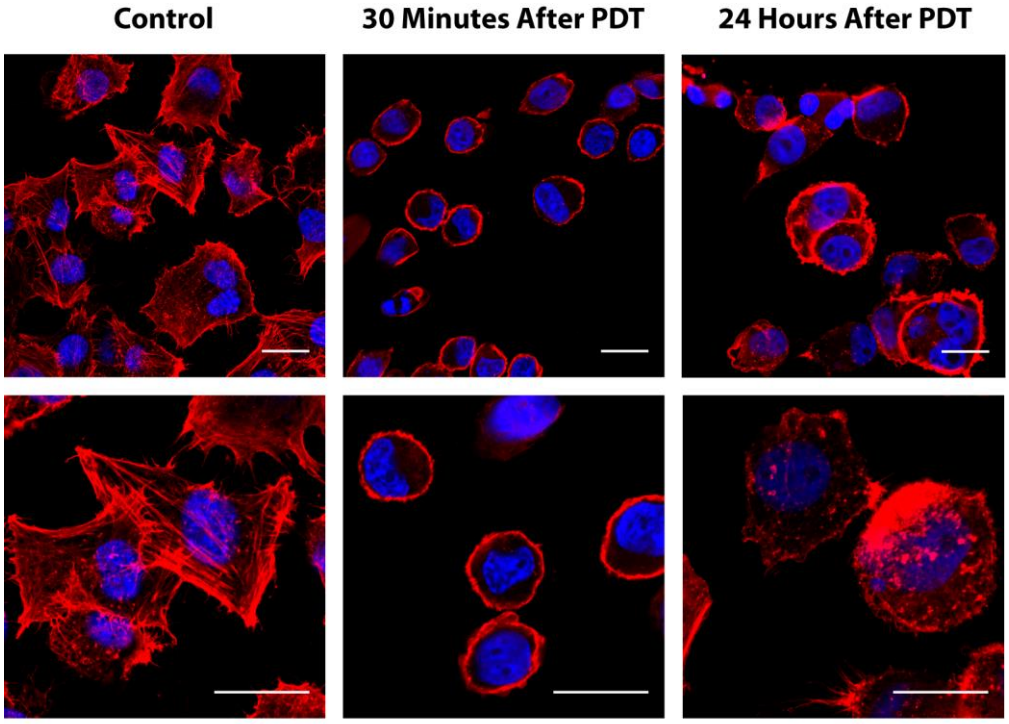

Figure 13. Changes of F-actin in UM-UC-3 cells 30 min and 24 h after targeted PDT with PorGal$_8$. Phalloidin-TRITC visualization of F-actin (red). The nuclei were stained with DAPI (blue). Scale bars 20 μm.

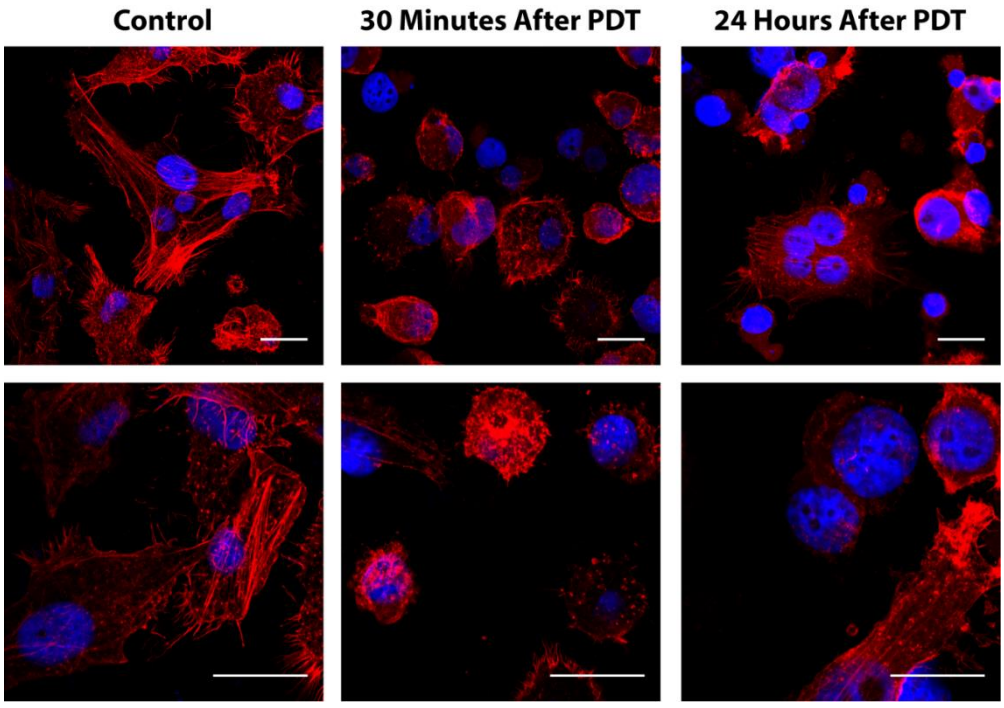

Figure 14. Changes of F-actin in HT-1376 cells 30 min and 24 h after targeted PDT with PorGal$_8$. Phalloidin-TRITC visualization of F-actin (red). The nuclei were stained with DAPI (blue). Scale bars 20 μm.

RhoA is a protein belonging to RhoA GTPases family involved with a multitude of cellular processes including, but not limited to, cell division, actin cytoskeleton regulation and induction of formation of stress fibers and focal adhesion points. In order to evaluate whether cytoskeleton changes and cell death are correlated with changes in RhoA protein levels, Western blot analysis was performed. Preliminary data showed that RhoA protein levels were not altered in UM-UC-3 cells 30 min or 24 h after PorGal$_8$-PDT (Fig. 15A). Interestingly, RhoA protein levels showed a tendency towards an increase in HT-1376 cells twenty-four hours after PorGal$_8$-irradiation (Fig. 15B).

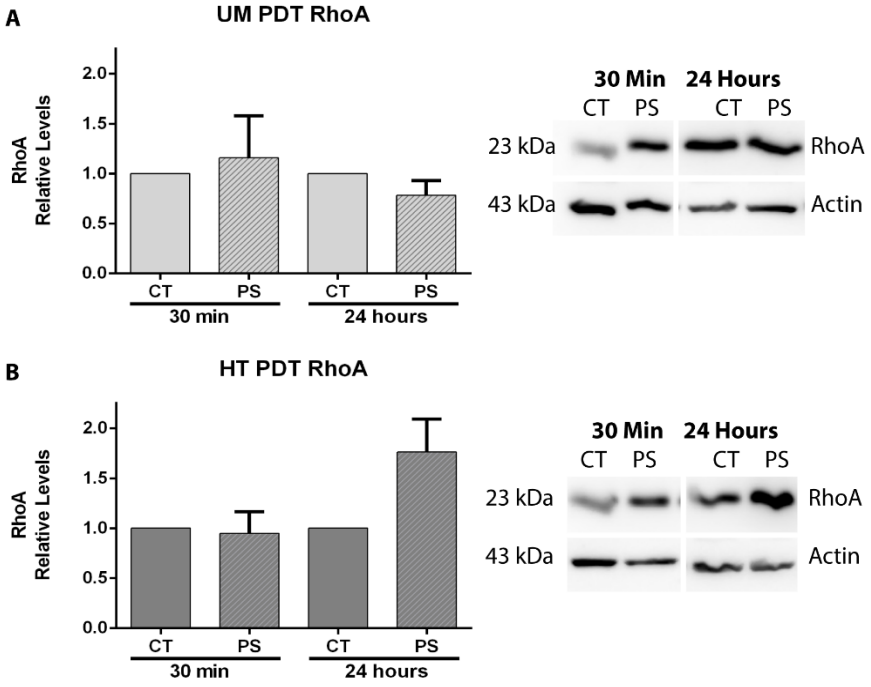

Figure 15. Western Blotting analysis and quantification of RhoA expression in UM-UC-3 (panel A) and HT-1376 (panel B) cell lines thirty minutes and twenty-four hours after irradiation. β-actin was blotted as loading control. Quantitative analysis of RhoA (normalized to β-actin) expressed as ratio to levels found in control cells (cells incubated with PBS instead of PorGal$_8$) in UM-UC-3 and HT-1376 cell lines. Data represents the mean ± S.E.M. of at least three independent experiments in UM-UC-3 cell line. Preliminary results from UM-UC-3 cell line do not present significant alteration in RhoA levels. HT-1376 cell line shows increase in the expression of RhoA twenty-four hours after irradiation-PorGal$_8$.

Chapter 5. Discussion

Many photosensitizers exist in the market and although their potential as anti-cancer drugs used in PDT is well established, the exact mechanisms underlying their phototoxic effects are relatively unknown. The major mechanisms described in PDT that activate cell death indicate that a diverse set of different pathways can be activated, being dependent, among other factors, on the cell line, light fluence rate and photosensitizer (Castano et al. 2005; Ball et al. 2001).

Current available PS lack enough tumor selectivity, which can cause side effects in the healthy surrounding tissues. Many efforts have been made to develop novel PS with tumor selectivity, by conjugation with biomolecules, such as carbohydrates (Zheng et al. 2011; Vedachalam et al. 2011; Lourenco et al. 2014).

A galactodendritic porphyrin ($PorGal_8$) had been engineered (at QOPNA, Department of Chemistry, University of Aveiro) to possess four dendritic units of galactose attached as dimeric units to a porphyrin which confers benefits in PDT. In fact, $PorGal_8$ had shown improved water solubility, high photo stability, the ability to induce the production of oxygen singlet, and improved selectivity to tumor cells, by interaction with galectin-1 that is overexpressed in bladder cancer (Pereira et al. 2016; Cindolo et al. 1999).

More recently, we have validated $PorGal_8$ as a novel therapeutic agent for the treatment of tumours exhibiting high levels of galectin-1. We have shown a specific uptake of this PS and induction of ROS-mediated cell death (Pereira et al. 2016).

This study was designed to evaluate whether changes in cytoskeletal components are correlated with cell death triggered by PDT with $PorGal_8$. Uptake studies showed a concentration-dependent intake of $PorGal_8$ in the cell lines, with maximum reached at 10-12.5 μM. At 10 μM, UM-UC-3 cell line possessed a higher uptake, of at least 5-fold compared to HT-1376 cell line. The higher $PorGal_8$ uptake in UM-UC-3 cells can be explained by the high expression of galectin-1 (Pereira et al. 2016; Camby et al. 2002). In fact, *in vitro* studies from our laboratory have shown preferential accumulation of $PorGal_8$ in cancer cells overexpressing galectin-1, accompanied by high phototoxicity. Also, by knockdown galectin-1 protein in bladder cancer cells, we have also found a significant decrease of PS uptake and phototoxicity, suggesting the role of galectin-1 in $PorGal_8$ selectivity (Pereira et al. 2016).

As expected, we found that $PorGal_8$ did not induce cell death in the dark. However, twenty-four hours after photodynamic activation, $PorGal_8$ induced a significant decrease in cell viability in both cell lines, assessed by MTT colorimetric and Trypan Blue assays. $PorGal_8$ led to a higher cytotoxicity after PDT in UM-UC-3 cells (approximately 50%) than in HT-1376 cells

(approximately 20%). Our previous studies have shown that although a strong phototoxic effect was observed at 72 h after treatment in UM-UC-3 cells, a certain percentage of HT-1376 cells are able to recover from the photodynamic effect between 24 and 72 h after $PorGal_8$ photoactivation (Pereira et al. 2016).

It is known that cell adhesion to the substratum is mediated by integrins and other cellular adhesion molecules that connect the extracellular matrix to the intracellular actin cytoskeleton. Moreover, it has been thoroughly studied the effect of PDT in the actin filaments.

Although adhesion proteins and actin filaments have been subject of various studies, the changes induced after PDT are highly variable with different effects reported. Due to this, the cytoskeleton changes induced after PDT are considered to be dependent on cell line, fluence rate and photosensitizer (Ball et al. 2001).

Microtubules have already been reported to play a key role in cell movement. Moreover, α-tubulin changes are involved in the motility of intracellular structures, such as the endoplasmic reticulum and actin filaments (Lee et al. 1995). A tendency towards a decrease in α-tubulin protein levels thirty minutes after irradiation was observed in both tested cell lines. HT-1376 cells presented a network rearrangement to a round shape. In our study, we found that changes in α-tubulin levels only became significant twenty-four hours after irradiation in HT-1376 cell line where a significant protein level decrease is observed. Microtubules present reorganization with high reduction of staining and recovery of cellular shape similar to control. These reorganization of α-tubulin indicates an effort of HT-1376 cells in recovering from PDT.

Intermediate filaments are one of the least studied structures in PDT mediated alterations, although their main component, vimentin, has been reported to increase in PDT-treated cells. Our results did not show any significant alterations in the levels of vimentin thirty minutes after irradiation. However, a significant decrease in vimentin protein levels was found twenty-four hours after irradiation was observed in both cell lines. Although not statistically significant, the tendency towards an increase in vimentin protein levels thirty minutes after irradiation in HT-1376 cells could be taken as an indicator of cells trying to counteract the treatment. HT-1376 presented a small increase in protein levels, with retraction of vimentin network from the cell edge thirty minutes after treatment. UM-UC-3 presented a small decrease in protein levels. Twenty-four hours after, the statistical significance of the decrease in the protein levels was more accentuated in UM-UC-3 cell line. HT-1376 cells staining was highly decreased or nearly absent, with very few cells still presenting vimentin staining. We can hypothesize that the

difference obtained for vimentin protein in these two bladder cancer cell lines could be related to different resistance exhibited by the two cell lines to the phototoxic effect.

Actin filaments, the most widely studied structures in PDT induced cytoskeleton alterations, presented similar disorganization thirty minutes after irradiation with complete loss of actin stress fibres in both cell lines. Twenty-four hours after irradiation however, HT-1376 cell line presented signs of recovery with reorganization of actin filaments and formation of new stress fibres. Furthermore, long extensions, like large filopodia, were observed. These observations allow us to speculate that the higher sensitivity of UM-UC-3 cells are due to a deeper, irreversible effect. In HT-1376 cells however, resistance to therapy can be associated with a recovery in actin filaments.

Considering the various changes assessed in the cytoskeleton structures, it can be hypothesized that F-actin is not the only responsible for PDT efficiency and morphology changes, but a complex series of events that involve other cytoskeleton structures such as intermediate filaments and microtubules play a role in PDT effectiveness or resistance. Seemingly negligible alterations of tubulin and vimentin levels combined with subcellular redistribution after irradiation can afterwards dictate different treatment outcomes. Further studies, evaluating changes after the evaluated period, adhesion proteins variations or the effect of multiple PDT sessions should be evaluated in order to further understand the cellular behaviour and whether the effectiveness of the treatment can be increased.

It is known that galectin-1 is involved in cell motility and cytoskeleton organization via the Gal-1-induced expression of RhoA (Camby et al. 2002). As previous work from our laboratory reported high levels of galectin-1 in UM-UC-3 cells, it was of interest to evaluate whether RhoA protein levels changes after PDT with $PorGal_8$. Preliminary results showed no changes in the levels of RhoA in UM-UC-3 cells. Interestingly, preliminary data showed a tendency towards an increase of RhoA in HT-1376 cell line twenty-four hours after photoactivation of $PorGal_8$. Further studies evaluating whether RhoA cellular redistribution are warranted in order to further elucidate the role of RhoA in PDT efficiency.

Our results indicate that a complex web of events occurs in cytoskeletal elements that can justify different outcomes of the treatment. This study shows that not only actin filaments are affected by PDT, but also intermediate filaments and microtubules present significant changes in response to photodynamic treatment. Further studies are necessary to understand how these mechanisms are triggered and their relation to other key proteins such as adhesion proteins and other GTPases family proteins.

In summary, the results presented in this dissertation provide a better understanding of the relationship between the phototoxic effects of $PorGal_8$ and the disorganization of the cytoskeleton structure. Rearrangements of the actin, vimentin and α-tubulin cytoskeleton and changes in RhoA protein levels observed in this work may play an important role regulating cell death triggered by PDT with $PorGal_8$. Clarifying the mechanisms underlying PDT efficiency might contribute to envisage new potential therapeutic adjuvants for PDT, acting on the cytoskeleton, to treat resistant cancers.

Chapter 6. Conclusions

UM-UC-3 cell line proved to be have higher uptake and increase sensitivity to PDT with $PorGal_8$.

Cytoskeleton alterations accessed that distinct alterations in protein levels and protein relocation after PDT variate, with a seemingly recovery in HT-1376 cell line. Microtubules suffer reorganization but changes in protein levels are only observed in HT-1376 twenty-four hours post-irradiation. Intermediate filaments although suffering similar reduction in protein levels twenty-four hours after irradiation, alterations immediately after PDT indicate a first response that can dictate cellular resistance to PDT afterwards. In actin filaments, although a similar preliminary response in disorganization and loss of stress fibers, HT-1376 presents signs of recovery with short stress fibers and long extensions, like large filopodia.

Preliminary results show an increase in RhoA levels in HT-1376 twenty-four hours after treatment, indicating a more complex web of events unfolding that the one previously presumed.

We proved that cytoskeleton alterations cover a wider series of structures that the ones usually described, with indication that statistically negligible alterations immediately after irradiation may play a role in later survival. Briefly, we believe this is the first work that tries to connect a wider series of cytoskeleton alterations with PDT efficiency and cell death.

Chapter 7. References

Agarwal, M.L. et al., 1993. Phospholipase activation triggers apoptosis in photosensitized mouse lymphoma cells. *Cancer Research*, 53(24), pp.5897–5902.

Almeida, R.D. et al., 2004. Intracellular signaling mechanisms in photodynamic therapy. *Biochimica et biophysica acta*, 1704(2), pp.59–86.

Assefa, N. & Yosief, T., 2003. Human Anatomy and Physiology. *Ephti*, p.428.

Ball, D.J. et al., 2001. Decreased efficiency of trypsinization of cells following photodynamic therapy: evaluation of a role for tissue transglutaminase. *Photochemistry and photobiology*, 73(1), pp.47–53.

Bekelman, J.E. et al., 2013. Radical cystectomy versus bladder-preserving therapy for muscle-invasive urothelial carcinoma: Examining confounding and misclassification biasin cancer observational comparative effectiveness research. *Value in Health*, 16(4), pp.610–618.

Belichenko, I., Morishima, N. & Separovic, D., 2001. Caspase-resistant vimentin suppresses apoptosis after photodynamic treatment with a silicon phthalocyanine in Jurkat cells. *Archives of biochemistry and biophysics*, 390(1), pp.57–63.

Bergamini, C. et al., 2004. Oxygen, reactive oxygen species and tissue damage. *Current Pharmaceutical Design*, 10(14), pp.1611–1626.

Bonnett, R. & Berenbaum, M., 1989. Porphyrins as photosensitizers. *Ciba Foundation Symposium*, 146, pp.40–53.

Van Den Bosch, S. & Witjes, J.A., 2011. Long-term cancer-specific survival in patients with high-risk, non-muscle-invasive bladder cancer and tumour progression: A systematic review. *European Urology*, 60(3), pp.493–500.

Bryan, R.T. et al., 2010. Mechanisms of recurrence of Ta/T1 bladder cancer. *Annals of the Royal College of Surgeons of England*, 92(6), pp.519–524.

Bugaj, A.M., 2011. Targeted photodynamic therapy – a promising strategy of tumor treatment. *Photochemical & Photobiological Sciences*, 10(7), pp.1097–1109.

Buytaert, E. et al., 2008. Molecular effectors and modulators of hypericin-mediated cell death in bladder cancer cells. *Oncogene*, 27(13), pp.1619–29.

Calin, M.A. & Parasca, S. V., 2006. Photodynamic therapy in oncology. *Journal of optoelectronics and Advanced Materilals*, 8(9), pp.1173–1179.

Camby, I. et al., 2002. Galectin-1 modulates human glioblastoma cell migration into the brain through modifications to the actin cytoskeleton and levels of expression of small GTPases. *Journal of neuropathology and experimental neurology*, 61(7), pp.585–596.

Casas, A. et al., 2008. Disorganisation of cytoskeleton in cells resistant to photodynamic treatment with decreased metastatic phenotype. *Cancer Letters*, 270(1), pp.56–65.

Castano, A.P., Demidova, T.N. & Hamblin, M.R., 2004. Mechanisms in photodynamic therapy: Part one - Photosensitizers, photochemistry and cellular localization. *Photodiagnosis and Photodynamic Therapy*, 1(4), pp.279–293.

Castano, A.P., Demidova, T.N. & Hamblin, M.R., 2005. Mechanisms in photodynamic therapy: Part two - Cellular signaling, cell metabolism and modes of cell death. *Photodiagnosis and Photodynamic Therapy*, 2(1 SPEC. ISS.), pp.1–23.

Celli, J.P. et al., 2003. Imaging and Photodynamic Therapy: mechanisms, monitoring, and optimization. *Chemical Reviews*, 39(12), pp.1137–1150.

Chedgy, E.C.P., Black, P.C. & et al, 2016. Radical Cystectomy and the Multidisciplinary Management of Muscle-Invasive Bladder Cancer. *JAMA: The Journal of the American Medical Association*, 2(7), pp.855–856.

Chen, B. et al., 2002. Photodynamic therapy with hypericin induces vascular damage and apoptosis in the RIF-1 mouse tumor model. *International Journal of Cancer*, 98(2), pp.284–90.

Cindolo, L. et al., 1999. Galectin-1 and galectin-3 expression in human bladder transitional-cell carcinomas. *International Journal of Cancer*, 84(1), pp.39–43.

David, A., 2010. Carbohydrate-based biomedical copolymers for targeted delivery of anticancer drugs. *Israel Journal of Chemistry*, 50(2), pp.204–219.

Egner, J.R., 2010. AJCC Cancer Staging Manual. *JAMA: The Journal of the American Medical Association*, 304, p.1726.

Ferlay, J. et al., 2013. Cancer incidence and mortality patterns in Europe: estimates for 40 countries in 2012. *European journal of cancer*, 49(6), pp.1374–403.

Foote, C.S., 1991. Definition of type I and type II photosensitized oxidation. *Photochemistry and photobiology*, 54(5), pp.659.

Garg, A.D. et al., 2010. Photodynamic therapy: illuminating the road from cell death towards anti-tumour immunity. *Apoptosis*, 15(9), pp.1050–71.

Gomer, C.J. et al., 1988. Molecular, cellular, and tissue responses following photodynamic therapy. *Lasers in Surgery and Medicine*, 8(5), pp.450–463.

Jodlbauer, A. & Von Tappeiner, H., 1904. Ueber die Beteiligung des Sauerstoffes bei der photodynamischen Wukung fluoreszierender Stoffe. *Deutsche Medizinische Wochenschr*, 52, pp.1139–1141.

Laemmli, U.K., 1970. Cleavage of structural proteins during the assembly of the head of bacteriophage T4. *Nature*, 227(5259), pp.680–685.

Lee, C., Wu, S.S. & Chen, L.B., 1995. Photosensitization by 3,3'-Dihexyloxacarbocyanine Iodide: Specific Disruption of Microtubules and Inactivation of Organelle Motility. *Cancer Research*, 55(10), pp.2063–2069.

Lourenco, L.M.O. et al., 2014. Amphiphilic phthalocyanine-cyclodextrin conjugates for cancer photodynamic therapy. *Chemical Communications*, 50(61), pp.8363–8366.

Luksiene, Z., 2003. Photodynamic therapy: mechanism of action and ways to improve the efficiency of treatment. *Medicina*, 39(12), pp.1137–1150.

MacDonald, I.J. & Dougherty, T.J., 2001. Basic principles of photodynamic therapy. *J. Porphyrins Phthalocyanines*, 5(2), pp.105–129.

Meyer-Betz, F., 1913. Untersuchungen uber die Biologische (photodynamische) Wirkung des hamatoporphyrins und anderer Derivative des Blut-und Gallenfarbstoffs. *Deutsche Medizinische Wochenschr*, 112, pp.476–503.

Mosmann, T., 1983. Rapid colorimetric assay for cellular growth and survival: application to proliferation and cytotoxicity assays. *Journal of Immunological Methods*, 65(1-2), pp.55–63.

O'Connor, A.E., Gallagher, W.M. & Byrne, A.T., 2009. Porphyrin and nonporphyrin photosensitizers in oncology: Preclinical and clinical advances in photodynamic therapy. *Photochemistry and Photobiology*, 85(5), pp.1053–1074.

Oleinick, N.L. & Evans, H.H., 1998. The photobiology of photodynamic therapy: cellular targets and mechanisms. *Radiation Research*, 150(5 Suppl), pp.S146–56.

Park, J.C. et al., 2014. Multimodal Management of Muscle Invasive Bladder Cancer. *Current Problems in Cancer*, 38(3), pp.80–108.

Pereira, P.M.R. et al., 2016. The role of galectin-1 in in vitro and in vivo photodynamic therapy with a galactodendritic porphyrin. *European Journal of Cancer*, 68, pp.60–69.

Pereira, P.M.R., Tome, J.P.C. & Fernandes, R., 2015. Molecular Targeted Photodynamic Therapy for Cancer. In *Handbook Porphyrin Science*. Vol. 4, pp. 1377–1386.

Plaetzer, K. et al., 2009. Photophysics and photochemistry of photodynamic therapy: Fundamental aspects. *Lasers in Medical Science*, 24(2), pp.259–268.

Pushpan, S.K. et al., 2002. Porphyrins in photodynamic therapy—A search for ideal photosensitizers. *Current Medicinal Chemistry - Anti-Cancer Agents*, 2(2), pp.187–207.

Ridley, A.J., 2003. Cell Migration: Integrating Signals from Front to Back. *Science*, 302(5651), pp.1704–1709.

Robertson, C.A., Evans, D.H. & Abrahamse, H., 2009. Photodynamic therapy (PDT): A short review on cellular mechanisms and cancer research applications for PDT. *Journal of Photochemistry and Photobiology B: Biology*, 96(1), pp.1–8.

Saladin, K., 2008. Human Anatomy. In *British medical journal*. pp. 727–728.

Separovic, D. et al., 2011. Combining anticancer agents photodynamic therapy and LCL85 leads to distinct changes in the sphingolipid profile, autophagy, caspase-3 activation in the absence of cell death, and long-term sensitization. *Biochemical and Biophysical Research Communications*, 409(3), pp.372–377.

Sharman, W.M., Allen, C.M. & Van Lier, J.E., 2000. Role of activated oxygen species in photodynamic therapy. *Methods in Enzymology*, 319, pp.376–400.

Silva, E.F.F. et al., 2010. Mechanisms of Singlet-Oxygen and Superoxide-Ion Generation by Porphyrins and Bacteriochlorins and their Implications in Photodynamic Therapy. *Chemistry - A Europpean Journal*, 16(30), pp.9273–9286.

Silva, S. et al., 2012. Porphyrin and phthalocyanine glycodendritic conjugates: synthesis, photophysical and photochemical properties. *Chemical Communications*, 48(30), p.3608.

Smith, P.K. et al., 1985. Measurement of protein using bicinchoninic acid. *Analytical Biochemistry*, 150(1), pp.76–85.

Soukup, V. et al., 2012. Follow-up after surgical treatment of bladder cancer: A critical analysis of the literature. *European Urology*, 62(2), pp.290–302.

Tanaka, T. et al., 2011. Pathobiology and chemoprevention of bladder cancer. *Journal of Oncology*, 2011(1), Article ID 528353, 23 pages.

Thijssen, V.L. et al., 2015. Galectin expression in cancer diagnosis and prognosis: A systematic review. *Biochimica et biophysica acta*, 1885(2), pp.237–47.

Thompson, D.B. et al., 2015. Immunological basis in the pathogenesis and treatment of bladder cancer. *Expert review of clinical immunology*, 11(2), pp.265–79.

Towbin, H., Staehelin, T. & Gordon, J., 1979. Electrophoretic transfer of proteins from polyacrilamide gels to nitrocellulose sheets: procedure and some applications. *Proceedings of the National Academy of Sciences USA*, 76(9), pp.4350–4354.

Uzdensky, A. et al., 2005. The effect of sub-lethal ALA-PDT on the cytoskeleton and adhesion of cultured human cancer cells. *Biochimica et Biophysica Acta - General Subjects*, 1722(1), pp.43–50.

Vedachalam, S. et al., 2011. Glycosylated porphyrin derivatives and their photodynamic activity in cancer cells. *Medicinal Chemical Communications*, 2(5), pp.371–77.

Venosa, G. Di, 2015. The role of cytoskeleton and adhesion proteins in the resistance to photodynamic therapy. Possible therapeutic interventions. *Photochemical & Photobiological Sciences*, 14(8), pp.1451–1464.

Vonarx, V. et al., 1995. Photodynamic therapy decreases cancer colonic cell adhesiveness and metastatic potential. *Research in Experimental Medicine*, 195(1), pp.101–116.

Witjes, J.A. et al., 2010. Hexaminolevulinate-Guided Fluorescence Cystoscopy in the Diagnosis and Follow-Up of Patients with Non-Muscle-Invasive Bladder Cancer: Review of the Evidence and Recommendations. *European Urology*, 57(4), pp.607–614.

Wojtyk, J.T.C. et al., 2006. Exploiting tumour biology to develop novel drug delivery strategies for PDT. *Medical Laser Application*, 21(4), pp.225–238.

Yau, T. et al., 2015. Lectins with Potential for Anti-Cancer Therapy. *Molecules*, 20(3), pp.3791–3810.

Zheng, G. et al., 2011. Synthesis of beta-galactose-conjugated chlorins derived by enyne metathesis as galectin-specific photosensitizers for photodynamic therapy. *The Journal of Organic Chemistry*, 66(26), pp.8709–16.